DIGITAL TERRAIN MODEL GENERATION USING STRUCTURE FROM MOTION: INFLUENCE OF CANOPY CLOSURE AND INTERPOLATION METHOD ON ACCURACY

by

Matthew Washburn, B.S.

A thesis submitted to the Graduate Council of
Texas State University in partial fulfillment
of the requirements for the degree of
Master of Science
with a Major in Geography
May 2017

Committee Members:

Jennifer Jensen, Chair

Kimberley Meitzen

Nathan Currit

FAIR USE AND AUTHOR'S PERMISSION STATEMENT

Fair Use

Duplication Permission

ACKNOWLEDGEMENTS

I would like to acknowledge all the help and support I received from my advisor, Dr. Jensen, as well as the other members of my committee.

I would also like to express my profound gratitude to my family and to my amazing wife for providing me with unfailing support and continuous encouragement throughout my years of study and through the process of researching and writing this thesis. This accomplishment would not have been possible without them. Thank you.

TABLE OF CONTENTS

Page

LIST OF TABLES

Table **Page**

LIST OF FIGURES

Figure **Page**

LIST OF ABBREVIATIONS

Abbreviation	Description
ALS	Airborne Laser Scanning
ANOVA	Analysis of Variance
ASPRS	American Society of Photogrammetry and Remote Sensing
ASTER	Advanced Space-borne Thermal Emission and Reflection Radiometer
ANN	Approximate Nearest Neighbor
CHM	Canopy Height Model
DTM	Digital Terrain Model
DEM	Digital Elevation Model
DOD	DEM of Difference
FOSS	Free and Open Source Software
GCP	Ground Control Point
GIS	Geographic Information System
GPS	Global Positioning System
InSAR	Interferometric Synthetic Aperture Radar
LIDAR	Light Detecting and Ranging
MVS	Multi-View Stereo
NAIP	National Agriculture Imagery Program
NED	National Elevation Dataset
NIR	Near Infrared
NVA	Non-vegetated Vertical Accuracy
PDOP	Positional Dilution of Precision
PMVS	Patch-based Multi-View Stereo
RANSAC	Random Sample Consensus
RMSE	Root Mean Square Error
SIFT	Scale Invariant Feature Transform
SfM	Structure from Motion
SRTM	Shuttle Radar Topography Mission
TIN	Triangulated Irregular Network
TLS	Terrestrial Laser Scanning
TNRIS	Texas Natural Resources Information System
USGS	United States Geological Survey
VVA	Vegetated Vertical Accuracy

1. INTRODUCTION

1.1 Background

The topographic structure and form of the Earth's surface plays an integral role in modulating atmospheric, geomorphic, hydrologic, and ecological processes occurring at multiple scales across the land surface. The strength of this relationship can directly inform our understanding of the nature and magnitude of these processes (Hutchinson and Gallant, 2000). Our ability to characterize and quantify these phenomena relies in large part on the ability to accurately represent topographic surfaces using land surface parameters such as slope, aspect, and curvature. These primary parameters directly influence many surface processes including: precipitation and temperature regimes, overland and subsurface flows, evapotranspiration and water budgets, spatial distribution and abundance of flora and fauna, and solar insolation (Wilson, 2012).

Interpreting the interaction and movement of water and energy across the Earth's surface is critical to understanding and modeling landscape response to various natural phenomena. High quality, high resolution bare earth digital elevation models (DEMs) are necessary inputs for a diverse array of applications including crop growth and precision agriculture (Bishop and McBrattney, 2002; Ouadrago, 2014), contaminant transport and runoff (Shen et al., 2013; Wang et al., 2015), forest management and biomass estimation (Vega and St. Onge, 2009; Maguya et al., 2014), wildfire modeling (Mutlu et al., 2008), hydrodynamic flood modeling and natural hazards (Tarekegn et al., 2010;), erosional dynamics (Karatson et al., 2012), and habitat suitability models (Sesnie et al., 2008; Kuebler et al., 2016). As this list continues to expand, it will be necessary to refine and test current methods of generating bare earth DEMs in order to more accurately calculate

primary and secondary land surface parameters (e.g., slope, aspect, roughness, flow-path, etc.).

Currently, highly accurate DEM products may be obtained from a number of different sources employing a variety of collection methods and sensor types. For example, the Shuttle Radar Topography Mission (SRTM) collected a global elevation dataset using C-band and X-band interferometric synthetic aperture radar (InSAR) over 11 days in 2000 (Hensley et al., 2007). The 90-meter product has near-global coverage (60˚N to 58˚S), with average vertical and horizontal accuracies of 16 meters and 20 meters, respectively. Due to its higher spatial resolution, the 30-meter product had a narrower ground track, only recording every second path. This resulted in reduced coverage for the same area, but with improved horizontal accuracies of 6 meters (Nelson et al., 2009).

Another frequently used DEM product is the Advanced Space-borne Thermal Emission and Reflection Radiometer (ASTER) Global DEM (GDEM). Launched in December 1999, the sensor is located onboard the Terra satellite as part of NASA's Earth Observing System and collects stereopair images from two near infrared (NIR) cameras which are combined photogrammetrically to produce a global DEM product (83˚N to 83˚S) (Nelson et al., 2009; DeWitt et al., 2015). Published in 2009, with a 30-meter spatial resolution, it was validated globally by NASA at 25-meter vertical accuracy (Chirico et al., 2012). Another commonly available elevation product is the National Elevation Dataset (NED). The NED is a living dataset which is updated bimonthly with the best available DEM data taken from multiple sources. It is the primary elevation dataset produced by the United States Geological Survey (USGS) and provides basic

elevation information for Earth science studies and mapping applications in the United States and most of North America in a seamless raster format (Gesch et al., 2014). Nationwide coverage is available at a 30-meter resolution, with 10-meter and 3-meter products being added as they become available - increasingly from lidar and other high-resolution sources. The accuracy of the NED varies spatially due to the variable quality of the source DEM, with the accuracy inherited from the original source (Maune, 2007). The overall absolute vertical accuracy is 1.55 meters, making the 30 meter products useful for regional mapping and the 3-meter product useable for more detailed studies (Gesch, 2007).

Because of their global coverage, the SRTM DEMs and the ASTER GDEM products may not meet the spatial resolution requirements for a small study area. Another major limitation is the temporal resolution of these products. The SRTM data were collected in 2000, potentially reducing usefulness in change detection analysis (DeWitt et al., 2015). Additionally, both products represent surface models only and must be further processed in order to derive a bare-earth model. The NED DEMs are more suited to regional and larger-scale analysis, but due to the variable sources, quality and accuracy issues can limit the scope and scale of their usefulness (Gesch, 2007; Gesch et al., 2014).

In view of the increasing number of data sets and the demand for such products, it is necessary to ascertain the performances and reliability of the different data sources of Digital Terrain Model (DTM) generation (Isioye and Jobin, 2011). Moreover, the proliferation of software packages using different DEM/DTM generation and filtering algorithms requires more information about the performance of these methods under different landscape conditions to better inform the choice of data source and DTM-

generation method. In order to choose the best filtering and interpolation methods for scientific and commercial users, it is therefore essential to assess various approaches of DEM production and achieved accuracies (Isioye and Jobin, 2011; Deilami and Hashim, 2011).

For clarity, the term "DEM" is defined here as a general model for representing elevation, and the "bare earth" modifier implies elevations of the terrain *only*, without vegetation or human-made features (i.e., a DTM) (Maune, 2007). Although DTMs can be created using different methods, the generalized workflow is the same. It begins with data capture, continues with data preprocessing and DEM generation, and concludes with filtering of vegetation and human-made structures. The resulting DTM can then be used to calculate land surface parameters of interest (Wilson, 2012).

DEM-generation can be accomplished using data obtained from ground surveys or remote sensing techniques. Ground survey DEMs are created by taking a series of elevation measurements using a total station or with a Global Positioning System (GPS) receiver. The points can then either be used to create a Triangulated Irregular Network (TIN) mesh that represents the elevation information, or the values between points can be interpolated using various algorithms resulting in a continuous surface or gridded raster. DEMs generated with manual ground survey techniques are highly accurate with errors less than 1 centimeter. The technique is also scalable to the study area and requires very minimal post-processing once the initial measurements have been recorded. However, the initial survey requires expensive equipment, intensive human effort, and can be very time-consuming (Nelson et al., 2009).

DEMs created from remote sensing sources are produced from a variety of data

sources and processing techniques. Traditionally, photogrammetry was employed to generate high resolution DEMs. Photogrammetry relies on extracting elevation information from high-resolution, high-quality photographs taken from airborne platforms. Broadly, photogrammetry operates by combining at least two overlapping 2D photographs into a 3D stereo-model using triangulation to compute the location of a point in all three dimensions. This requires *a priori* knowledge of the camera position and scene geometry for all photos in a set. In the case of DEM generation, the mosaicked aerial photographs are then georeferenced using ground control points (GCPs) of a projected coordinate system, and elevation information can then be extracted (Nelson, 2009).

The first commercial topographic mapping systems to use light detection and ranging (lidar) appeared in the early 1990s, and their popularity has grown rapidly in the last decade. Lidar systems rely on active transmission of a NIR signal to the surface of interest. The return of that signal is then recorded, and the distance to the surface is calculated by the time delay. Depending on the sensor, this can occur up to 250,000 times per second. A system clock on the sensor records the time each reflected pulse returns and a range to target is calculated. The range data are then combined with the GPS positions to calculate X, Y, and Z coordinates for each return and a 3D point cloud can then be generated (Nelson, 2009). Provided that the sensor is capable of processing discrete returns, the point cloud can further be classified into ground and non-ground returns, with the ground returns representing the DTM (Nelson, 2009). The capability to generate multiple surface models, along with the high point density and centimeter-level vertical accuracy, are responsible for lidar's increasing popularity and widespread

adoption over the past decade (Wilson 2012).

Airborne (ALS) and terrestrial-based (TLS) lidar surveying is currently the standard for accuracy and precision of measurement and has revolutionized the quality of DEMs, extending their spatial extent, resolution, and accuracy (Westoby et al., 2012; Dandois and Ellis, 2010). While highly precise and accurate, these methods can be prohibitively expensive due the high capital cost of equipment, bulky sensors, and extreme cost of tasking commercial aircraft to fly over a study area (Dandois and Ellis, 2010; Westoby et al., 2012). Moreover, these products are often purchased from a third-party vendor, and may not meet the spatial and temporal requirements of the researcher (Fonstad et al., 2013). Another approach to generating high density 3D point clouds as a low-cost alternative to lidar-based point clouds is Structure from Motion (SfM).

SfM offers a new method for DEM generation that incorporates many images taken from multiple perspectives. Using a suite of automated image-matching algorithms, a 3D lidar-like point cloud is derived, which can then be used to develop DEM and DTM products for the researcher's study area. The SfM technique is capable of delivering high-resolution 3D point cloud products at multiple spatial and temporal scales.

Initially conceived and developed by the computer vision community as a method for three-dimensional modeling of buildings, SfM is a highly accurate alternative to traditional lidar platforms in geographic investigation and research (Fonstad et al., 2013; Westoby et al., 2012). SfM works on the same general principle of stereoscopic photogrammetry that derives three-dimensional structure from a series of overlapping, offset images. It differs substantially, in that it is not necessary to establish the dimensional location of the camera *a priori*. This is accomplished by an image-matching

algorithm that iteratively reconstructs scene geometry by tracking relative camera position from image-to-image and by automatically matching features present in multiple images (Westoby et al., 2012; Snavely, 2008).

Ground Control Points (GCPs) with known geographic positions are then used to georeference the resulting point-cloud. The SfM method is best suited to imagery with a high degree of overlap taken from many different camera positions, which is usually accomplished from a moving sensor (Westoby et al., 2012; Dietrich, 2016). Images may be acquired in several ways, including the use of inexpensive, lightweight platforms like unmanned aerial vehicles (UAVs) which are gradually becoming more commonplace (Dandois and Ellis, 2010; Dandois et al., 2015; Fonstad et al., 2013; Westoby et al., 2012; Dietrich, 2016).

SfM techniques have been used to derive DEMs in a diverse range of environments. Applications including estimating forest canopy heights (Dandois and Ellis, 2013; Dandois et al., 2015, Wallace et al., 2016), predicting vineyard Leaf Area Index (Mathews and Jensen, 2013), monitoring coastal erosion in a beach dune system (Mancini et al., 2013), mass balance estimation in glaciers (Piermattei et al., 2014), and change detection in fluvial and riverine environments (Fonstad et al., 2013; Javernick et al., 2014; Deitrich, 2016) have been studied, with varying levels of success.

All of these studies require highly precise and accurate DEMs and DTMs in order to perform scientific analysis. This data can be obtained from ALS/TLS, but the cost is often prohibitively expensive. Not only does this limit the spatial considerations of the study, the high cost of tasking lidar limits the temporal resolution as well. This can be especially problematic for environments that are sensitive to change on the scale of years,

such as forests. It is therefore essential to establish the conditions under which SfM is most appropriate in forested environments.

1.2 Problem Statement

Developing a DTM from an image-based point cloud for areas under dense canopy is an area of active research due to the difficulty of obtaining a suitable number of under-canopy images from multiple perspectives (White et al., 2013). Research that addresses the utility and effectiveness of low-cost imagery and associated point clouds is necessary to demonstrate under what landscape conditions these methods are applicable (Jensen and Mathews, 2016). Although a few published studies have demonstrated that SfM-derived point clouds can be used to generate a moderately accurate DTM under vegetation canopy, the current literature lacks information about which vegetation structural conditions facilitate generation of ground points required to achieve an accurate topographic surface.

1.3 Research Objectives

While the SfM approach has been successfully implemented in a variety of landscapes, areas of dense vegetation, such as woodland ecosystems present several unique challenges, and have not been well-studied. This study will examine the effect of canopy density on DTM accuracy. Specifically, the following research objectives will be addressed:

- Objective 1: Assess the accuracy of SfM-derived DTMs under various canopy closure densities and evaluate influence of interpolation method and spatial resolution on DTM accuracy.
- Objective 2: Document the limitations of SfM for DTM generation compared with a lidar-derived DTM.

1.4 Justification

The rapid advancement of commercial UAV technology and open-source image processing software is democratizing spatial data collection. When equipped with an off-the-shelf digital camera, consumer-grade UAVs have reached a degree of technical maturity that enable on-demand 'personal remote sensing' of landscapes at high spatial and temporal resolution (Dandois et al., 2015, Pirokka et al., 2015).

SfM offers several advantages over traditional photogrammetry and lidar including low cost, relative ease of use, and the ability to monitor vegetation and landscape dynamics in near real-time. Due to the growing popularity and use of SfM for geographic research, it is therefore necessary to test the capabilities under various conditions and document potential limitations of this emerging technology.

2. LITERATURE REVIEW

2.1 Overview of DEMs: History, Applications, and Data Structures

The ability to model a continuous topographic surface using automated methods was made possible by the advent of the digital computer in the 1950s. Relying heavily on postwar technological advances and innovation, modern terrain modeling began with trend surface analysis – a technique which uses a polynomial expression to interpolate surface values. Paralleling this method, Bonner and Schmall (1973) used spectral analysis to derive slope profiles for the Moon's surface through Earth-based photoclinometry, or "shape from shading" (Pike et al., 2009).

The modern DEM concept was first formally described in 1958 (Miller and Laflamme), but was not in common use until the 1960s. Due to computational limitations, most gridded DEMs were generally prepared by manual interpolation of existing contour maps, with semi-automated digitizing and production becoming more commonplace in the latter part of the decade. A major milestone occurred in 1968 when Pike and Wilson (1971) began to create the USGS's first DEMs and developed software to calculate land surface parameters (Pike et al., 2009).

The progress of digital computers through the 1970s and 1980s enabled the development of sophisticated and automated DEM generation and analysis techniques, and the wide availability of desktop computers in the 1990s facilitated more complex analysis in GIS software packages (Pike et al., 2009).

In order for a DEM to represent the land surface, it must be a complete and *continuous* surface from which heights for any location (i.e., points) must be calculable. In practice, this continuous surface may be represented and structured using one of two

data models: vector (irregular) or raster (regular) (Hengl and Evans, 2009). Each representational method is appropriate for different applications, and a brief overview is presented here.

A Triangulated Irregular Network (TIN) is a vector-based structure that is used to model irregularly spaced sampled points across a surface. TINs are constructed from this array of points by connecting each point to its two nearest neighbors. This results in a series of contiguous, non-overlapping triangles that forms a topographic mesh. Because this model uses a planar topology, areas of consistent elevation, slope, and aspect may be represented with the individual triangle facets (Maune, 2007; Hengl and Evans, 2009).

TIN-based models are generally more accurate in representing discrete changes over variable topography than raster-based models and are much more efficient at storing elevation data because they are able to adapt to the variable complexity of terrain (i.e., areas of low variation require less storage). However, the complex and variable nature of their data structure makes TINs less *computationally* efficient than raster-based formats. The vector-based structure of a TIN also supports incorporation of point, line, and polygon features which embeds the original source measurements in the network, allowing more accurate analysis by incorporating surface-specific features such as breaks, ridges, and course lines. This requires high quality data, high point density data (usually from photogrammetry or lidar), and can often be expensive to obtain (Maune, 2007; Hengl and Evans, 2009).

The raster-based, regular data model is more commonly used than the vector model and is usually represented in a regularly-spaced, square gridded format where each cell is attributed with elevation values that describe the land surface (Wilson, 2010). The

regular and consistent structure of raster-based DEMs is simpler than the variable, adaptive nature of a TIN. While raster-based DEMs are less efficient at data storage, their uniform spatial structure allows greater computational efficiency. This makes raster-based DEMs better suited to deriving land-surface parameters using common geomorphometric algorithms (Hengl and Evans, 2009). Moreover, the spatial resolution of raster-based DEMs can be easily resampled using simple interpolation methods.

Although they are much more commonly used, the raster-DEM has several disadvantages. Due to the regularly-spaced nature of the grid, areas of complex and variable terrain are under-sampled (i.e. the surface morphology is not accurately modeled). Reprojection of the data's coordinate system can introduce errors and result in a loss of accuracy (Hengl and Evans, 2009). Wilson (2010) notes that by reducing the unit of analysis from a variable surface to a gridded cell of discrete size, locally significant terrain features such as ridgelines and streams may be lost. The scale dependency of many surface features can also be problematic, especially when working with coarse DEMs. It is also important to note that while both raster and vector formats attempt to capture the topography of the land surface, they are *models* based on sampled points. The modeled surface is an estimation based on several factors including data collection method, ground sampling distance, point density, and interpolation method.

2.2 Lidar Applications in DEM Generation

The data sources and processing methods for generating DEMs have evolved rapidly over the past 20–30 years; from ground surveying and topographic map conversion, to passive methods of remote sensing, and more recently to active sensing

with lidar and radar (Wilson, 2010). Active systems such as lidar have a number of advantages over passive systems (e.g., photogrammetry). Lidar's capability to penetrate canopy gaps, coupled with the non-interference of shadow and sun angle on data acquisition, as well as the ability to process discrete returns with varying intensity attributes is contributing to its popularity for DEM/DTM generation (Liu, 2008). Additionally, the density of lidar point clouds enable generation of high accuracy, high resolution DEMs (Meng et al., 2010).

DEM generation from lidar has been shown to outperform photogrammetry in various environments, including forested areas. In a pioneering study, Kraus and Pfeifer (1998) performed an accuracy assessment on DTMs generated using lidar and photogrammetry in a 91 km^2 wooded area over in the Vienna Woods, Austria. With a 25 percent canopy penetration, the results established that the accuracy of the lidar-generated DTM (25 cm) in wooded areas was equivalent to photogrammetrically-generated DTMs in *open* areas. After the application of a filtering algorithm, the accuracy of the lidar-DEM was improved to 10 cm, demonstrating that lidar can deliver highly accurate DEM/DTM products in forested environments (Liu, 2008).

Another significant early study involved *automated* DEM-generation in urban and coastal areas, establishing that lidar-generated DEMs are highly accurate in different environments with variable terrain. Vertical accuracies of 10 cm were achieved, providing proof of concept of DEM utility for applications including water resource management, shoreline control, and urban planning (Lohr, 1998). In short, accurate DEM generation from lidar for various topographic conditions has since been thoroughly documented in the literature. The use of lidar for topographic modeling and DEM

generation is becoming the standard for accuracy, and is being adopted as the primary technique based on the capability to rapidly generate highly resolution DEMs over large areas (Meng et al., 2010).

2.3 The Structure from Motion Alternative

Perhaps the greatest disadvantage to the use of lidar-generated DEMs is the extreme cost. For smaller study areas, or for applications requiring dynamic monitoring such as forests, coastal environments, or fluvial systems, lidar can be prohibitively expensive (Piroka et al., 2015). The SfM technique has been demonstrated to be capable of delivering high resolution DEM products of similar accuracies as lidar-derived DEMs in various conditions. The general workflow is described here.

SfM is a non-selective survey method that captures a set of overlapping images taken from multiple viewpoints. While there are minor differences depending on the software package used, the general workflow is the same (Smith et al., 2016). First, features, or "keypoints" within each image are identified iteratively through the entire set of photographs. This is generally accomplished by implementing the Scale Invariant Feature Transform (SIFT) algorithm, which selects features in each image that are invariant to illumination, image scaling, and rotation (Lowe, 2004). Each image feature is recorded and assigned a unique descriptor consisting of a series of vectors locating each feature in the image set (Smith et al., 2016).

Next, keypoint matching is accomplished by matching the mathematical descriptors of features present in multiple images using the Approximate Nearest Neighbor algorithm (Arya et al., 1998). Keypoints are then filtered further in order to

eliminate erroneous matches using the Random Sample Consensus (RANSAC) method which randomly samples and tests candidate features for inclusion based on pairwise comparison (Fischler and Bolles, 1981). This method eliminates transient features that many be present in multiple images such as people, equipment, or objects on the sensor (Westoby, 2012).

After candidate keypoints are matched and filtered, sparse bundle adjustment algorithms (Snavely, 2008) simultaneously estimate 3D scene geometry and internal camera parameters (e.g. focal length, radial distortion, etc.) (Smith, 2016). This is different from traditional photogrammetry where camera parameters must be specified *a priori.* The resulting sparse 3D point cloud is unscaled and lacking a projected coordinate system.

The sparse point cloud is then georeferenced using a minimum of three GCPs with XYZ coordinates, although many more are recommended (Javernick et al., 2014). This can either be accomplished using direct georeferencing derived from a GPS measurement onboard the sensing platform, an indirect method obtained using ground targets with known coordinates, or a hybrid approach combining the two methods (Dandois and Ellis., 2015; Ryan et al., 2015; Smith, 2016).

The final step in the SfM workflow is the densification of the point cloud by applying Multi-View Stereo (MVS) algorithms to the sparse point cloud. MVS has been shown to increase the density of the point cloud by two orders of magnitude (Smith et al., 2016). A commonly used MVS algorithm in physical geographic applications is the Patch-based MVS (PMVS) method (Furukawa and Ponce, 2010), which operates by identifying and growing patches around keypoints based on image texture (Westoby,

2012; Smith, 2016). The end product is a georeferenced, dense 3D point cloud that can then be processed into a DEM, or filtered to a DTM.

2.4 Recent Studies Implementing SfM: Non-Vegetated Landscapes

DEMs and DTMs derived from image-based point clouds have been studied in several different environments, under a variety of landscape conditions, all supporting varied research goals. This review groups each study by the geomorphic environment it was performed in.

Fonstad et al. (2013) examined the applicability of SfM in the Pedernales River, Texas using a helikite to acquire low altitude imagery of a bedrock, fluvial environment. The study compared the agreement between SfM, GPS, and an existing lidar dataset in order to assess relative differences between data acquisition methods. A DEM of Difference (DOD) was created by subtracting the lidar-DEM from the SfM DEM. SfM-derived DEMs had point densities (10.8 points/m^2) far exceeding the lidar dataset (0.33 points/m^2), with centimeter-level horizontal and vertical accuracies. The mean horizontal difference of SfM and lidar orthometric heights was 0.27 meters (0.60 m vertical), and a regression of the SfM to lidar elevation values resulted in a 97 percent explanation of variance in the SfM dataset.

In the first quantified analysis of SfM applied to model a braided river, Javernick et al. (2014) performed a quality assessment of SfM and lidar-generated sub-meter DEM products along two contiguous reaches (1.7km and 1.6 km) of the Ahuriri River, New Zealand. The photographic dataset was acquired at 600 to 800 meters using a handheld digital camera. Results indicated that SfM is capable of delivering high quality terrain

datasets competitive with lidar with mean horizontal errors of 0.04 meters, and vertical errors of 0.10 meters in non-vegetated areas, creating a DTM suitable for geomorphic change detection and hydrodynamic modeling.

Westoby et al. (2012) examined the applicability of SfM in three different locations across a range of scales including an exposed rocky cliff, a breached moraine-dam complex, and a glacially sculpted bedrock ridge by comparing the derived DEMs with those acquired using TLS. Imagery was acquired with a handheld digital camera. The resulting point clouds were decimated to reduce computational demands, but the summary statistics were retained. A 1-meter grid was used to filter minimum elevation values for the DTM, and a DOD was created by subtracting the SfM model from the TLS model. Results indicated that while decimeter-scale vertical accuracy was achieved, areas of dense vegetation cover is problematic for effective terrain reconstruction due to the lack of heterogeneity of the image texture. Additionally, the point densities were limited, and "of questionable accuracy" under areas of dense vegetation. However, SfM is shown here to be an effective, low-cost, and dynamic method for modeling complex topography.

In a change detection analysis using SfM, Lucieer et al (2014) mapped landslide dynamics with a UAV platform. A 1-centimeter DEM was generated for two different dates five months apart, and then differenced in order to assess degree of offset for several areas, and an image correlation algorithm was applied to compute lateral displacement of the landslide features. After visual analysis using a write memory function insertion technique, it was determined that the SfM-derived DEM was able to accurately model surface changes over active landslides. GCPs were also collected with GPS in order to assess accuracy of the DEM products. Horizontal and vertical accuracies

of 0.07 meters and 0.06 meters were achieved, respectively.

2.5 Recent Studies Implementing SfM: Vegetated Landscapes

Dandois and Ellis (2010) deployed a kite equipped with a digital camera across two 2.25 ha test sites in Baltimore, MD to estimate various vegetation metrics using SfM. A 1-meter DTM was derived from the SfM data, and compared with an existing lidar-derived DTM to estimate Canopy Height Models (CHMs). Both point clouds were processed using a progressive morphological filtering algorithm (Zhang et al., 2003) to separate ground and non-ground points, and interpolated into a grid using Ordinary Kriging. Accuracies of 1.5 meters RMSE horizontal and 0.6 to 4.3 meters RMSE vertical were reported. Results also indicate that the SfM-derived point cloud had much lower point densities than the lidar point cloud, especially under tree canopy (0.02-0.03 points/m^2 for the SfM point cloud, compared to 0.4-0.6 points/m^2 for the lidar point cloud). These sparse point densities resulted in DTM errors, especially in vegetated areas.

The sparse densities under canopy for the SfM relative to the lidar can partially be accounted for given that the lidar data were acquired during leaf-off conditions, while the SfM images were captured during leaf-on conditions. The authors also note that the flight parameters were less than ideal, with images acquired at a low degree of overlap contributing to lower agreement between lidar and SfM datasets. Given these limitations, the CHMs derived from the SfM-DTM were still found to adequately predict field-measured tree heights ($R^2 > 0.64$), though lidar showed a greater precision ($R^2 > 0.82$).

Extending the scope of the previous analysis, Dandois and Ellis (2013) further examined the ability of SfM-derived DTMs to measure forest structure and spectral

dynamics. In addition to acquiring more recent and phenologically similar lidar data, widening the study area (three 6.25 ha sites), this analysis was performed with a stable UAV system capable of acquiring images at more optimal conditions. The point clouds were decimated using a 1-meter grid that retained only the median elevation value. The resulting point cloud was then further processed using the same morphological filter from the previous analysis (Dandois and Ellis, 2010). In a SfM workflow, the algorithm operates by identifying "ground" points based on elevation differences within user-defined kernel sizes around each point within a specified grid mesh (Zhang and Cui, 2007). Ordinary Kriging was then used to rasterize the point cloud into a 1-meter resolution DTM grid.

The improved methodology and image acquisition parameters resulted in point cloud densities ranging from 30-67 points/m^2 with the highest vertical precisions found under leaf-off conditions (RMSE 0.73 m to 2.72 m) compared with leaf-on acquisitions (3.37 m to 5.69 m). At two of the sites, the derived CHMs were found to be strong predictors of field-measured tree heights (R^2 = 0.63, and R^2 = 0.84) and were highly correlated with a lidar CHM (r = 0.87). These results indicate that leaf-off DTMs that are accurate to < 3 m RMSE are adequate for estimating forest canopy heights. While DTM accuracies are also reported by landcover type (e.g. Forest, Water, Turfgrass, Brush, Building, Pavement, Water, and Other), the canopy densities are not quantified. This presents a potential limitation of the study that requires further analysis.

Jensen and Mathews (2016) compared SfM and lidar-derived DTM products to assess accuracy and to estimate canopy heights in a woodland ecosystem. Images were acquired with a UAV flown at an altitude of 100 meters over a 15-ha study area. The

resulting SfM point cloud was first decimated using a 0.5-meter block minimum filter, then classified further using an adaptive TIN filtering algorithm. After a final manual classification, a 1-meter DTM was generated using a natural neighbor algorithm.

Final point densities of 2.58 points/m^2 (SfM) and 0.72 points/m^2 (lidar) were reported. DTM differencing analysis indicated that the SfM-derived surface overestimated the lidar-modeled ground height with a mean difference of 0.19 meters with a standard deviation of 0.66 meters. Spatial distribution of error values (i.e. difference between GPS and SfM elevation values at spatially coincident points) indicated that the SfM-derived DTM overestimated elevations in dense canopy and underestimated the ground surface in open areas.

Wallace et al. (2016) performed a simultaneous comparison of ALS and SfM point-cloud generation methods using a small UAV to assess forest structural characteristics from a 30-m x 50-m plot in a dry eucalyptus forest with spatially varying canopy cover. In order to facilitate direct comparison of methods, the UAV was equipped with both a laser scanner device (i.e. lidar) and a digital camera to capture high resolution photographs. Canopy cover was estimated for the entire plot (59 percent) from the point clouds of both datasets using a 2D alpha shape of all returns greater than 1.3 m. This algorithm reconstructs an object's shape from a set of random points with a user-defined threshold value (Edelsbrunner et al., 1994; Wallace, 2013). Cover was also calculated for a 0.5-m grid as a binary value and compared along two transects. LAStools, a commonly used software package used to filter lidar returns, was used to identify ground points. A 10-cm DTM was interpolated using an adaptive TIN algorithm. The point density of the ALS point cloud (174 points/m^2) was significantly less than the point density of the

SfM point cloud (5,652 points/m^2). However, under areas of canopy, the SfM underperformed ALS in capturing the terrain surface, resulting in point density of less than 1 point/m^2 and mean difference from ALS terrain surface of 0.12 m. These reported results indicate that SfM-derived DTMs consistently overestimate elevation values under canopy. This study used a novel method to directly estimate canopy cover from the point clouds for the entire study area, but is limited by only reporting canopy cover in binary values for the calculated 0.5-m grid. Further analysis should include a comparison of ALS and SfM-generated DTMs at specific, quantified canopy closure values.

3. MATERIALS AND METHODS

3.1 Study Area and Site Selection

The study area is located on a section of the Freeman Center - a 1,400 hectare Texas State University-managed ranch and research facility - northwest of San Marcos, TX (29° 94’ N, 97° 99’ W). Situated along the eastern edge of the Edwards Plateau in the Balcones Canyonlands Ecoregion in Central Texas, the area is characterized by rugged to moderately flat stair-step topography. The underlying karstic geology results in thin, ustic soils with drainages consisting of low-gradient bedrock-dominated ephemeral streams surrounded by densely vegetated riparian zones.

Land cover is primarily woodlands and shrublands with some grassland areas cleared and managed for grazing. Woodland vegetation includes plateau live oak (*Quercus fusiformis*), Texas oak (*Quercus buckleyi*), Ashe juniper (*Juniperus asheii*), and cedar elm (*Ulmus crassifolia*). Grasslands are minimally distributed with little bluestem (*Schizachyrium scoparium*), yellow Indiangrass (*Sorghastrum nutans*), and sideoats grama (*Bouteloua curtipendula*) present. (Griffith et al., 2007). Mean annual precipitation ranges from 660 - 863 mm. Mean January temperatures range from 0-15 degrees Celsius and mean July temperatures range from 21-34 degrees Celsius. The area is characterized by a high degree of climatic variability and subject to a wide variety of conditions indicative of a humid sub-tropical climate (Dixon, 2000).

Research was conducted across several of the pastures covering 22 hectares on the southeastern side of the Ranch, near the Williamson-Freeman Dam.

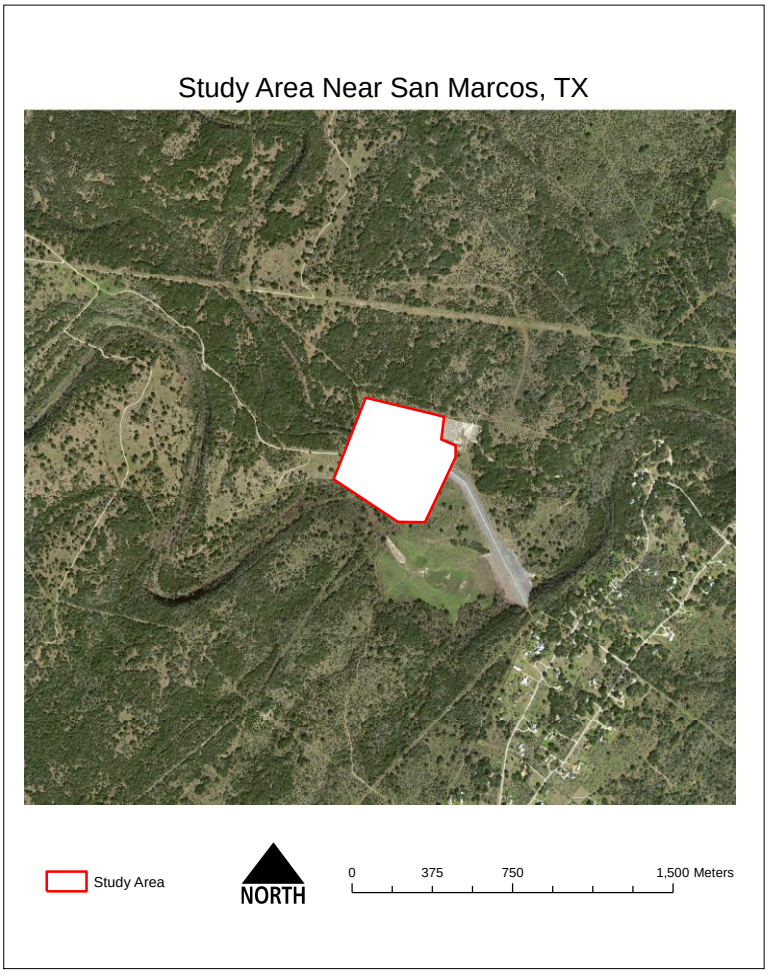

Figure 1: Study Area

A total of thirty 10-m x 10-m candidate plots representing increasingly dense canopy cover were identified using the 30-meter 2011 National Landcover Dataset (NLCD) percent canopy cover product. Of these initial candidate plots, twenty-eight were selected for this study using 4-band National Agriculture Imagery Program (NAIP) imagery acquired during leaf-on conditions in 2015. This resulted in six plots representing non-vegetated terrain, and twenty-two plots representing canopy densities ranging from 10-100 percent cover. The location of each plot centroid was then used to

plan image acquisition and UAV flight parameters.

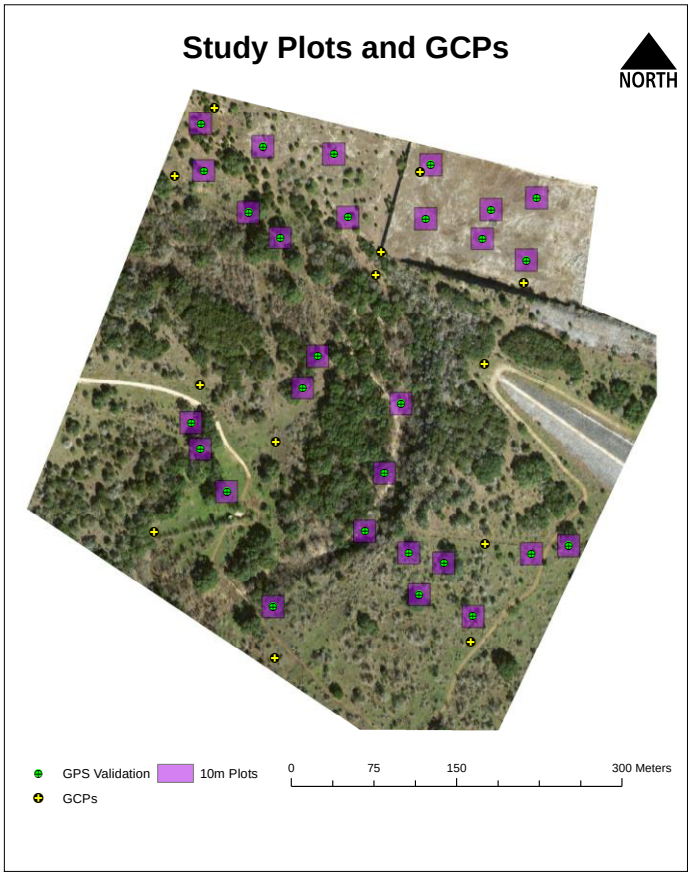

Figure 2: Plots and GCP Locations

3.2 Image Acquisition

Twelve 0.5-meter diameter, high-contrast Ground Control Points (GCPs) were placed preflight throughout the study area, and their locations were recorded using a Trimble GeoXH GPS receiver with an external Zephyr antenna. Positional Dilution of Precision (PDOP) was set to a maximum of 3.0 and vertical and horizontal precisions of 0.15 meters and 0.17 meters, respectively were achieved after differential correction.

Aerial imagery of the study area was acquired on October 28, 2016 between 11:00

am and 1:00 pm. Weather conditions were overcast early, with passing clouds in the afternoon. Light wind from the SSE made for favorable flight conditions. A 3D Robotics X8+ UAV system was used to collect aerial imagery using a GoPro Hero3+ camera mounted at nadir, set to capture images at 1-second intervals. Due to UAV battery limitations, it was necessary to divide the study area into four sections, requiring three separate takeoff and landing sites. Flight parameters were programmed using Mission Planner software, and written to the UAV's autopilot system, with takeoff and landing operations handled manually. Following recommendations from Dandois et al. (2015) to maximize point density and canopy gap penetration, image overlap parameters were set to 80 percent sidelap and 90 percent forward overlap. Flight altitude was kept below 40 meters for each flight.

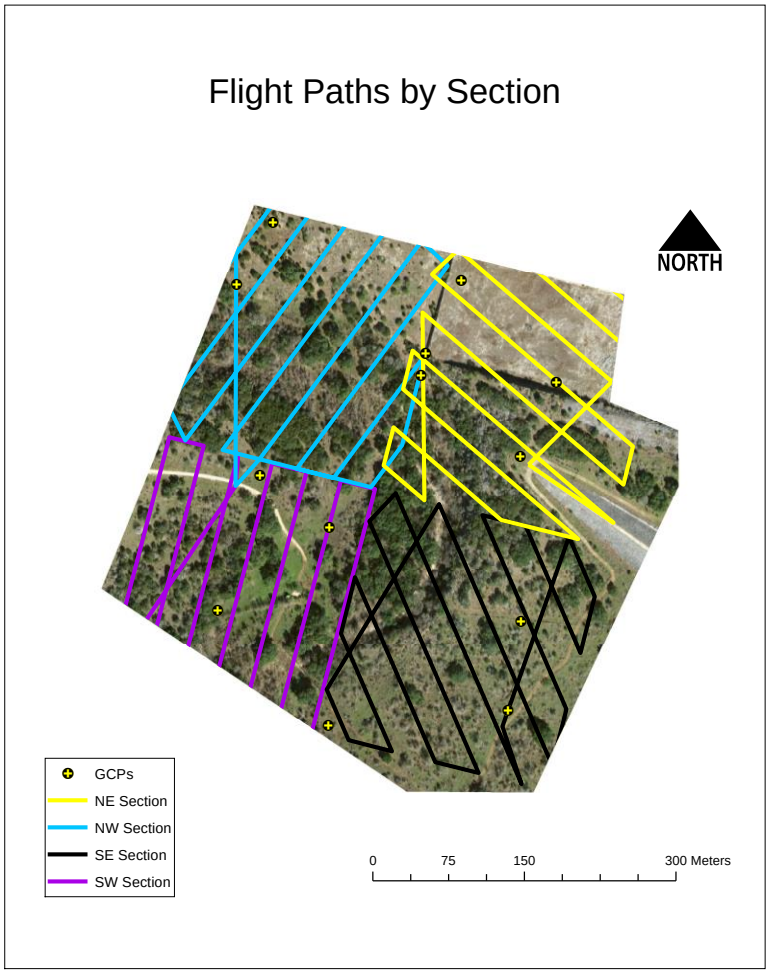

Figure 3: Flight paths for each section and corresponding GCPs

A previously acquired lidar dataset of the study area was used to assess the accuracy of the SfM-generated DTM. The lidar data were acquired in 2008 and made available by the Texas Natural Resource Information System (TNRIS).

3.3 Canopy Closure Estimates

Canopy cover refers to the proportion of the ground that is covered by the vertical projection of tree crowns (Jennings et al, 1999), and was used to identify and select

candidate plots with 2011 NLCD canopy cover product along with high-resolution NAIP imagery. Field measurements of canopy density were then estimated using the canopy closure metric, or the proportion of the sky hemisphere obscured by vegetation when viewed by a single point (Jennings et al., 1999; Egan, 2010).

Canopy closure measurements were estimated during leaf-on conditions on November 5, 2016 at points roughly coinciding with the centroids of the twenty-eight candidate plots established using the NLCD and NAIP products. The final 10-meter plot boundaries were defined from this position, which was recorded using GPS with a maximum PDOP value of 4.0 and mean vertical and horizontal precisions of 0.15 meters and 0.13 meters, respectively. While the GPS receiver was logging positions (300 per plot center), canopy closure was estimated using two different methods.

First, measurements were taken facing each cardinal direction with a spherical densiometer held at approximately 1 meter above the ground and 0.5 meters in front of the GPS antenna. Readings were captured using a 12-megapixel iPhone 6s camera, and calculated afterward, using the mean value of all four readings.

Figure 4: Spherical densiometer reading canopy closure

Next, the same GoPro camera used for aerial image acquisition was used to take hemispherical photographs of the sky above each plot centroid. As with the densiometer, photos were taken facing the cardinal directions, at the same height and distance. The mean canopy closure value for each plot was calculated using a free digital image analysis program developed by the US Forest Service called ForestCrowns (Winn et al., 2016).

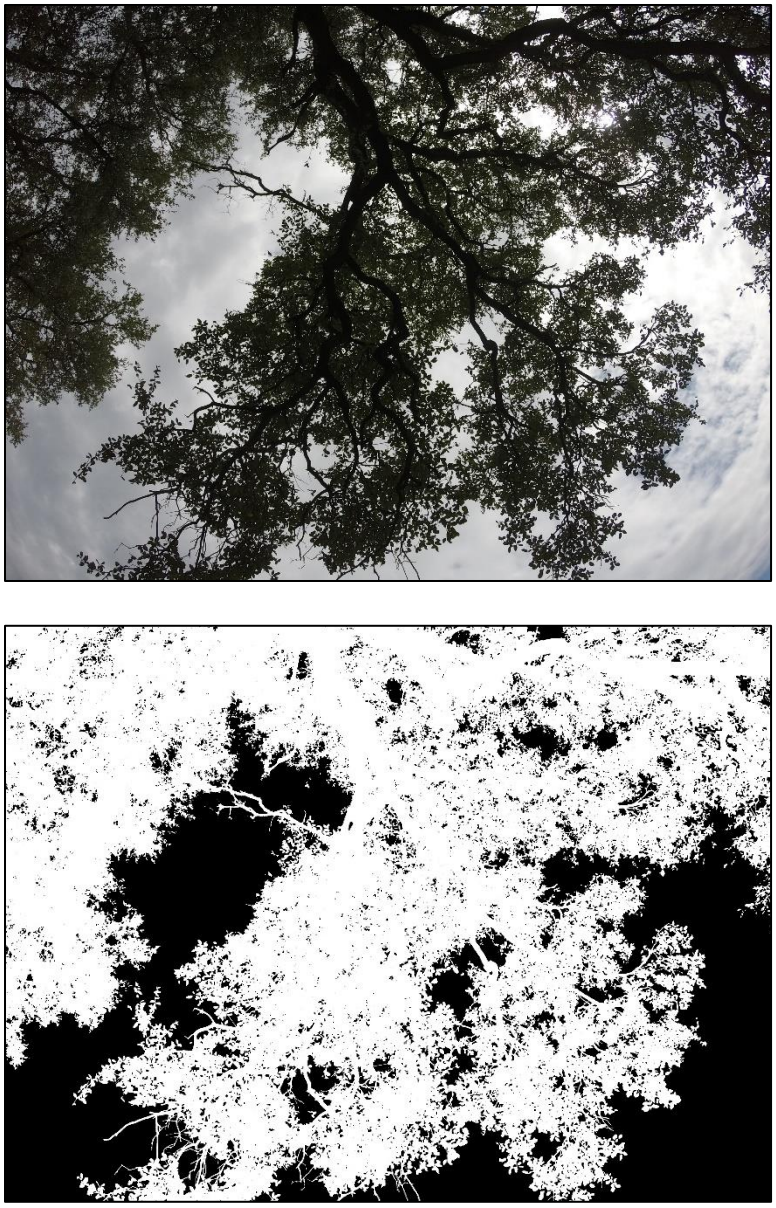

Figure 5: Hemispherical photographs of canopy pre- (top) and post-processing (bottom)

While there was moderate agreement between both estimates (r = 0.93) the hemispherical photography method provided a more consistent, repeatable, and appropriate method for canopy closure estimates than the spherical densiometer technique and is therefore used for canopy closure measurements in this study.

For the twenty-two vegetated plots, canopy closure estimates ranged from 12-78 percent. Using a Jenks/natural breaks classification system, the plots were grouped into four categories representing increasing canopy cover: Very Low (12-26 percent), Low (27-41 percent), Medium (42-65 percent), and High (66-78 percent). The Very Low and Low classes consist of five plots per class, and the Medium and High consist of six plots per class. The American Society of Photogrammetry and Remote Sensing (ASPRS) accuracy standards require separate calculations for vegetated and non-vegetated areas, so the six non-vegetated plots were not included in this classification scheme.

3.4 Image Processing and Point Cloud Generation

A total of 2,767 total images were collected over the 22-hectare study area. Of those, 671 images were rejected for poor image quality, off-nadir angle, motion blur, or duplication. The remaining 2,096 images were loaded into Agisoft Photoscan for processing. Due to the large number of images, the project was split into four separate "chunks" (sections) corresponding to flight sections (NE, SW, SE, NE). Although this helped reduce computational demand, each chunk still required a significant amount of processing time. An overview of the processing workflow for each chunk is presented below.

First, all images were automatically calibrated using the Exchangeable Image File Format (EXIF) tags associated with them. This information includes the camera focal length and radial distortion parameters, and allows the software to minimize error in the resulting model.

Next, all images within the set were aligned using the "High" setting for the

"Accuracy" parameter, with all other parameters set to the default values. Image alignment is necessary for estimation of image position and orientation, and builds a sparse point cloud by identifying keypoints present within multiple images. After the sparse cloud was generated, a dense point cloud was reconstructed based on calculated depth information for each image in the set. Reconstruction parameters available for adjustment are "Quality" and "Depth Filtering Mode", which were set to "High" and "Aggressive", respectively. These are the recommended values for processing aerial imagery.

After dense point cloud reconstruction, a 3D mesh surface was generated with the parameters "Surface type" set to "Height Field" and "Source Data" set to "Dense Cloud", and all other parameters set to their default values. The height field surface type is optimized for modeling of planar surfaces and is recommended for processing aerial imagery of terrain.

Reconstruction of a 3D mesh surface facilitated automated georeferencing using "Guided Placement" of GCP markers. Using this feature, each GCP marker was placed in a single photo, and the corresponding ray was projected onto the model surface. This automatically calculates the GCP location on each photo in the set where the GCP is present, and speeds up marker placement by requiring only fine manual adjustments in corresponding photos. This approach was chosen due to the large number of photos, and to minimize the chance of incorrect GCP marker placement.

After the point cloud was georeferenced using the GCPs into a projected coordinate system (WGS 1984 UTM 14N), the four chunks were then aligned and merged using the GCPs as points of reference. The resulting unclassified dense point

cloud represents a DSM, and required further processing including classification and decimation.

Table 1: Point cloud metrics by section

Section	Images	GCPs	Sparse Cloud	Dense Cloud	Point Density	Point Spacing	RMS Reprojection Error	Processing time
NE	446	4	162,505	87,627,971	505 points/m²	4.5 cm	0.49 m	31 hrs
SE	505	4	360,995	139,048,739	796 points/m²	3.5 cm	0.53 m	35 hrs
SW	431	4	306,686	137,667,754	799 points/m²	3.5 cm	0.44 m	25 hrs
NW	714	6	415,402	152,453,040	961 points/m²	3.2 cm	0.47 m	74 hrs
Full	**2096**	**12**	**1,262,794**	**516,758,301**	**772 points/m²**	**3.6 cm**	**0.48 m**	**165 hrs**

3.5 Ground Classification and Decimation

The workstation used for this project had the following specifications: Windows 7 Enterprise PC 64-bit, SSD, Intel Core i7 CPU 870 @ 2.93 GHz, 16 GB RAM, NVIDIA Quadro NVS 420 GPU 2 GB RAM. However, attempts to apply a classification algorithm to the full, dense point cloud were unsuccessful due to lack of computational resources. Instead of classifying the entire dense point cloud, each chunk was classified separately using a morphological filtering algorithm with the following parameters: "Maximum Angle" = 15 degrees, "Maximum Distance" (above model surface) = 0.5 meters, and "Cell Size" = 30 meters (for all except the NE chuck where "Cell Size" = 20 meters). The algorithm operates within the "Cell Size", or window value, iteratively classifying points as ground only if the vertical distance between the point and the 3D

model surface is less than 0.5 meters *and* the angle between the nearest point is less than 15 degrees. In order to minimize errors of commission (i.e. non-ground classified as ground), the window size was set to the largest area of contiguous non-ground points in each chunk based on visual inspection of the dense cloud. The resulting ground points were then exported as separate LAS files for decimation and further manual classification.

Next, the four aligned sections (chunks) were imported into CloudCompare, a Free and Open Source Software (FOSS) application and decimated with a minimum point spacing of 0.5 meters. This helped reduce demand on computational resources, and allowed for more detailed visual examination of the point clouds. Further removal of obvious outliers in the point clouds was accomplished using a *k*-means spatial resample.

The algorithm operates by computing the mean distance of each point to its neighbors, considering *k*-nearest neighbors, then rejects points that are farther than the average distance plus a number of times the standard deviation ($d_{max} = d_{\mu}$ + nSigma * std dev). All points that are greater than the maximum distance are then rejected. In order to avoid overly aggressive outlier removal, values of k = 10, and nSigma = 1.0 were chosen.

Iterative application of this algorithm to all sections thinned the point clouds to more computationally manageable sizes and allowed the aligned, georeferenced, ground-classified sections to be merged and exported into a single LAS file, and finally a point shapefile (using the LP360 extension for ArcGIS) with 364,739 points and a mean density of 1.65 points/m^2 over the entire 22-hectare study area.

Figure 6: Unclassified decimated SfM point cloud

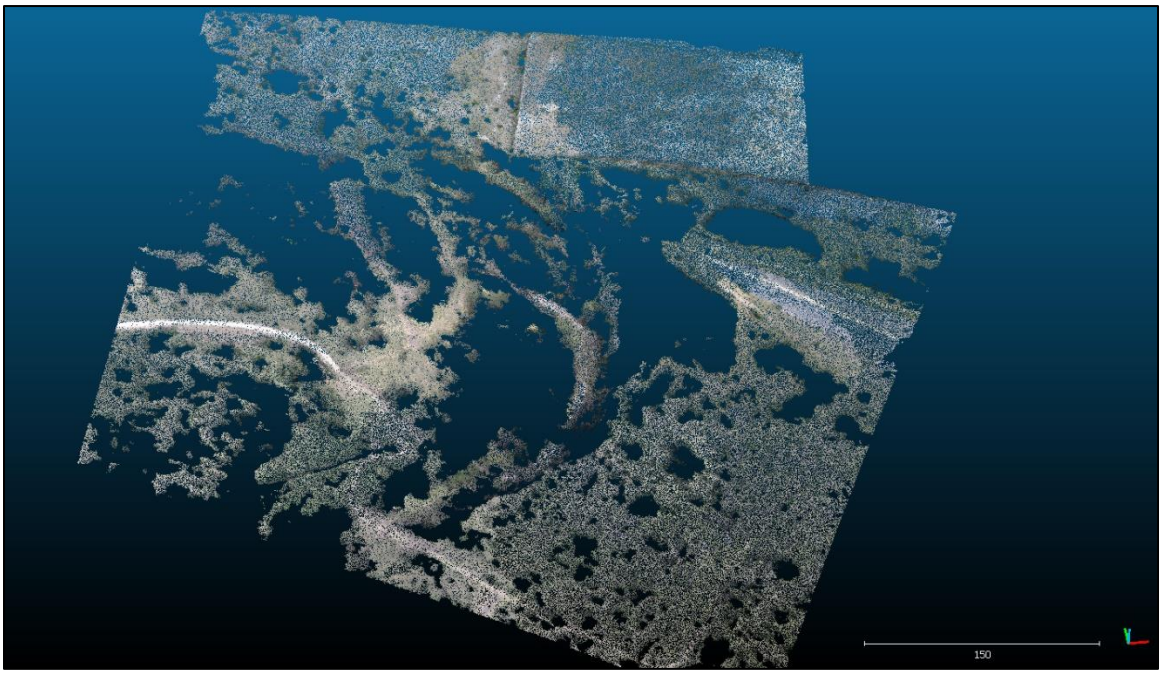

Figure 7: Ground-classified decimated SfM point cloud

3.6 DTM Generation

After the existing lidar dataset was reprojected from NAD83 State Plane Texas S Central 4204 into WGS84 UTM 14N using LAStools, ground points were exported to a point shapefile using the extent of the SfM dataset as a boundary. Four DTMs were generated in ArcMap for both the SfM and lidar shapefiles using Natural Neighbor and Ordinary Kriging interpolation methods at different spatial resolutions. Natural Neighbor DTMs were interpolated or both datasets at spatial resolutions of 50 centimeters, 1 meter, and 2 meters. Ordinary Kriging was used to generate a 1-meter DTM for both datasets.

The raster surface values of the resulting eight DTMs were then sampled and extracted at each of the twenty-eight GPS-measured plot centroids (GPS validation point). The GNSS height was subtracted from the raster surface, and the results were exported to Microsoft Excel to calculate absolute error, total Root Mean Squared Error (RMSE), ASPRS Non-Vegetated Vertical Accuracy (NVA) at the 95% confidence level, and Vegetated Vertical Accuracy (VVA) at the 95^{th} percentile.

RMSE is a measure of the total error present between observed measurements (e.g. GPS validation points) and predicted values (e.g. spatially coincident DTM surface), and is reported in meters.

For vertical accuracy testing, different methods are used in non-vegetated terrain and vegetated terrain. In non-vegetated areas, errors typically follow a normal distribution suitable for RMSE statistical analyses. Vertical errors are not necessarily normally distributed over vegetated terrain and cannot be represented parametrically. In these areas, the 95^{th} value more fairly estimates accuracy at a 95% confidence level.

The NVA at the 95% confidence level in non-vegetated terrain is approximated

by multiplying the accuracy value of the RMSE by 1.9600. The VVA at the 95% confidence level in vegetated terrain is computed as the 95th percentile of the absolute value of vertical errors in all vegetated land cover categories combined, including tall weeds and crops, brush lands, and fully forested areas. For all vertical accuracy classes (i.e. predetermined accuracies in centimeters) the VVA standard is 3.0 times the accuracy value of the class or the RMSE (ASPRS, 2015). The RMSE is reported in this study.

4. RESULTS

4.1 DTM Accuracy Assessments

Extracting the difference between the DTM height (DTM_Z) and the GPS orthometric height (GPS_Z) enabled calculation of both degree and direction of error (i.e. overestimation or underestimation of ground surface) between the SfM models (DTM_{SfM}), the lidar models (DTM_{lidar}), as well as the total RMSE, NVA, and VVA for each DTM.

Table 2: Accuracy assessment for SfM and lidar DTMs

DTM	Total RMSE (meters)	NVA 95% Confidence (meters)	VVA 95th Percentile (meters)
lidar NN 50cm	1.15	2.18	1.65
SfM NN 50cm	1.64	1.42	3.73
lidar NN 1m	1.14	2.18	1.65
SfM NN 1m	1.64	1.42	3.73
lidar NN 2m	1.15	2.17	1.64
SfM NN 2m	1.54	1.39	3.81
lidar Krig 1m	1.15	2.19	1.63
SfM Krig 1m	1.58	1.41	3.84

The most accurate DTM_{lidar} (i.e. the lowest RMSE) was generated using Natural Neighbor (NN) at a spatial resolution of 1-meter, and the most accurate DTM_{SfM} was generated using NN at a 2-meter spatial resolution. While this 2-meter NN DTM_{SfM} had slightly higher VVA error than the 1-meter DTM_{SfM}, both the RMSE and NVA are lower than at other spatial resolutions. All DTM_{lidar} were more accurate on vegetated surfaces,

and all DTM_{SfM} were more accurate on non-vegetated surfaces, however the DTM_{lidar} were much more *consistent* predictors of observed elevation values.

Figures 8 and 9 plot the fit between the elevation values of each GPS validation point and the elevation value for the nearest lidar or SfM point. The linear fit is displayed in blue, and the 1:1 line is dashed.

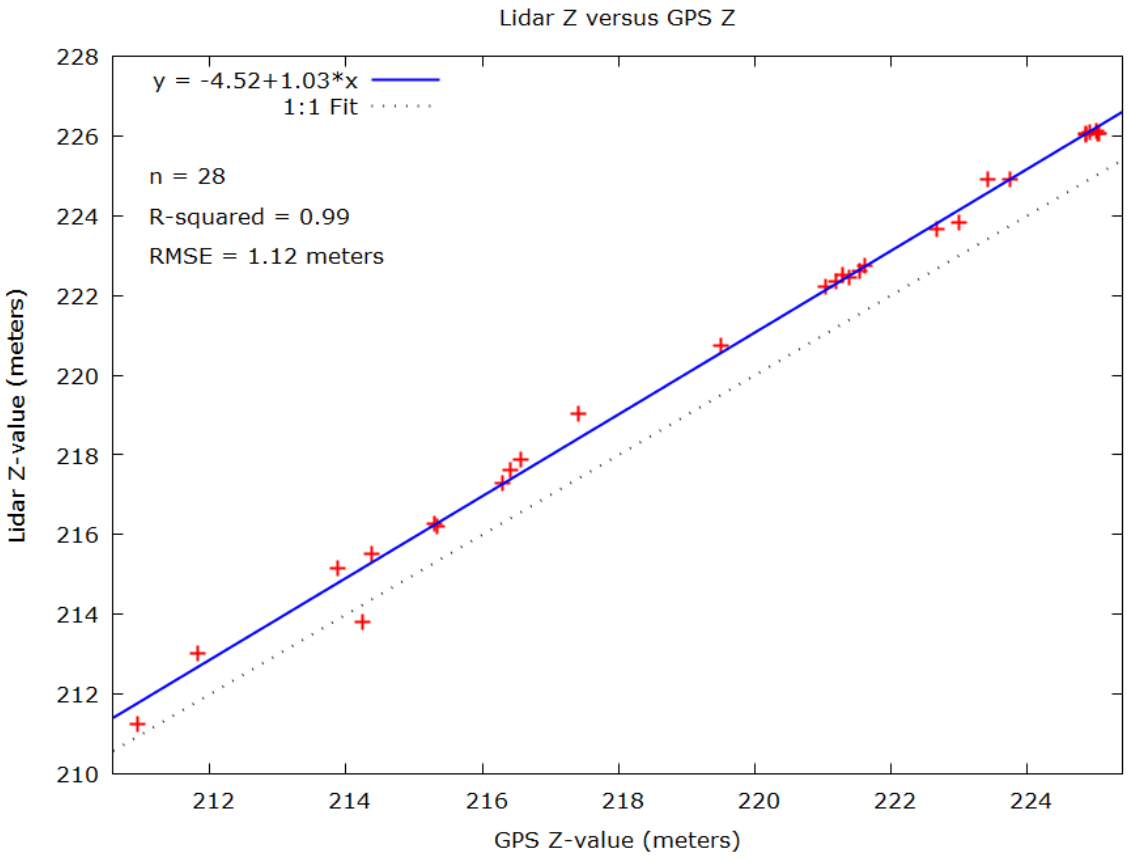

Figure 8: OLS fit between lidar elevation and GPS orthometric heights

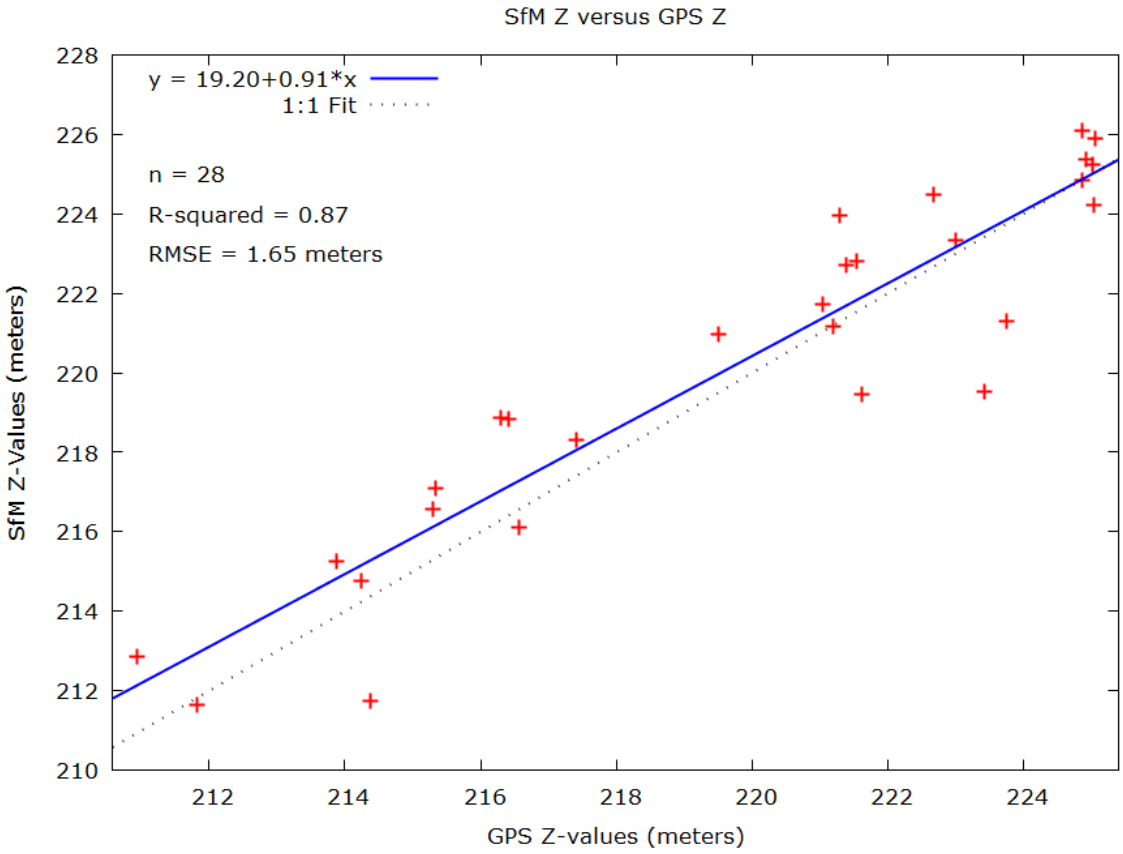

Figure 9: OLS fit between SfM elevation and GPS orthometric heights

While the lidar point cloud displayed greater agreement between observed and predicted heights (R^2 = 0.99) than the SfM point cloud did (R^2 = 0.87), it consistently overestimated the GPS_Z (mean error = 1.06 meters, RMSE = 1.12 meters). The SfM cloud was a more inconsistent predictor of GPS_Z (mean error = 0.45 meters, RMSE = 1.65 meters), exhibiting greater model agreement at higher elevations, and less agreement at lower elevations. Regression of spatially coincident SfM and lidar points across the entire study area reveals moderate agreement (R^2 = 0.78) between both datasets, and displays greater agreement at higher elevations. This may be the result of the non-

vegetated plots' location, along an emergency spillway, which is at a higher elevation than the rest of the study area.

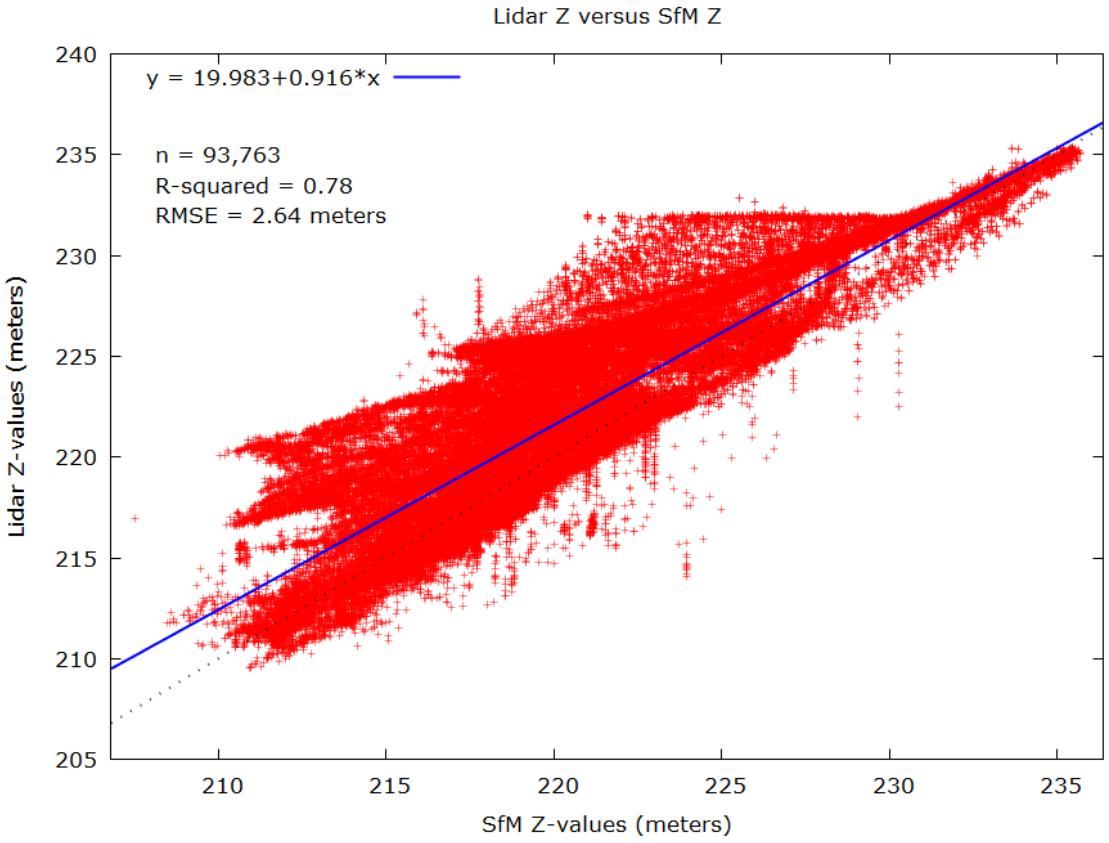

Figure 10: OLS fit between SfM and lidar ground-classified points

4.2 Plot Metrics and Statistical Analysis

Table 3 displays plot statistics for both SfM and lidar point clouds as well as DTM-derived values for each 10 x 10-meter plot slope and slope at GPS validation points. Canopy closure estimates are included for reference, and are spatially coincident

with the slope at GPS validation points. Slope values were calculated using the 1-meter DTM_{lidar} NN surface, and are reported in degrees. Elevation values are reported in meters, and canopy closure estimates are ranked in ascending percent closure.

Table 3: Plot statistics for lidar and SfM clouds

Plot ID	SfM Point Count	Lidar Point Count	Mean SfM Z	Mean Lidar Z	SfM Z Range	Lidar Z Range	Mean Plot Slope	Slope at GPS Point	Canopy Closure at GPS Point
9	1,090	273	225.04	226.11	1.92	0.41	1.68	0.98	0
15	624	274	224.36	226.07	1.19	0.34	1.40	1.23	0
21	714	279	226.22	226.09	1.17	0.37	1.33	0.54	0
25	606	262	225.54	226.11	0.99	0.35	1.25	0.95	0
26	622	261	226.07	226.11	0.97	0.35	1.43	1.22	0
28	619	256	225.33	226.11	1.10	0.40	1.39	1.48	0
4	689	282	222.64	222.46	0.87	0.52	1.50	1.19	12
3	697	205	220.92	220.73	2.90	3.03	7.01	6.50	16
13	598	174	221.08	222.32	1.94	0.43	2.08	3.02	17
19	1,624	185	216.67	217.75	2.67	1.60	4.74	5.50	18
27	638	234	222.87	222.64	1.11	0.48	1.56	0.51	26
24	708	228	221.37	224.91	2.28	0.55	1.95	1.10	32
1	396	96	221.97	222.30	2.32	1.28	2.58	1.42	37
2	571	129	224.50	223.70	2.29	1.47	3.88	2.32	39
18	1,263	238	222.84	222.38	3.48	1.70	4.08	3.78	41
5	1,310	86	218.04	218.81	3.97	1.18	2.74	3.96	41
17	342	79	223.65	223.93	1.96	1.34	3.53	2.54	55
0	321	90	219.61	224.97	3.09	0.80	2.50	6.14	56
16	519	152	218.91	217.36	1.54	0.49	2.15	2.78	59
11	674	223	219.68	222.65	1.82	1.18	2.45	1.06	63
22	868	202	215.33	215.58	5.88	0.58	1.99	0.70	64
29	773	105	215.64	216.41	4.34	0.93	2.90	3.37	65
10	450	88	213.21	211.41	3.47	4.01	13.68	9.38	69
14	895	115	212.94	213.20	5.60	1.85	5.63	3.52	72
12	976	171	215.72	216.27	7.04	3.49	8.86	10.82	74
7	369	69	214.26	213.34	6.84	3.60	10.02	13.33	74
6	565	178	218.97	217.83	1.82	1.79	4.45	2.51	74
8	520	98	215.33	215.04	3.02	3.36	8.46	7.22	78

Tables 4 and 5 display plot statistics for both SfM and lidar point clouds grouped into the previously established canopy closure classification system. As with Table 3 above, elevation values are extracted directly from the ground-classified point clouds. Nominal canopy closure values were assigned an integer rank for analysis. Mean point density represents the total point count for each canopy class divided by the total area covered by that class, and is reported in points/m^2.

Table 4: Canopy closure class statistics for SfM point cloud

Canopy Closure Class	Canopy Rank	Number of Plots	Point Count	Mean Density	Mean Z	Range Z	Std Dev Z
Non-vegetated	1	6	4,275	7	225.40	3.49	0.65
Very Low	2	5	4,246	8	219.89	8.49	2.67
Low	3	5	4,248	8	221.26	9.70	2.46
Medium	4	6	3,497	6	217.97	13.36	2.92
High	5	6	3,775	6	215.05	11.71	2.24

Table 5: Canopy closure class statistics for lidar point cloud

Canopy Closure Class	Canopy Rank	Number of Plots	Point Count	Mean Density	Mean Z	Range Z	Std Dev Z
Non-vegetated	1	6	1,605	3	226.10	0.47	0.07
Very Low	2	5	1,080	2	221.34	5.87	1.81
Low	3	5	777	2	222.94	6.78	1.82
Medium	4	6	851	1	219.62	10.22	3.64
High	5	6	719	1	215.12	8.78	2.28

Figures 10 and 11 plot the fit between mean point density and canopy closure rank for both lidar and SfM ground-classified points. While canopy closure is a good predictor of mean point density of the lidar dataset ($R^2 = 0.93$), the relationship is much weaker between the SfM ground points and the canopy closure ranks ($R^2 = 0.31$). The canopy closure density does not appear to significantly influence the density of SfM ground-classified points. This may be a result of the morphological filtering algorithm used to classify the SfM point cloud. The relatively high SfM point densities under both Very Low (8 points/m^2) and Low (8 points/m^2) may also be responsible for the apparent lack of influence by canopy closure when grouped into these classes.

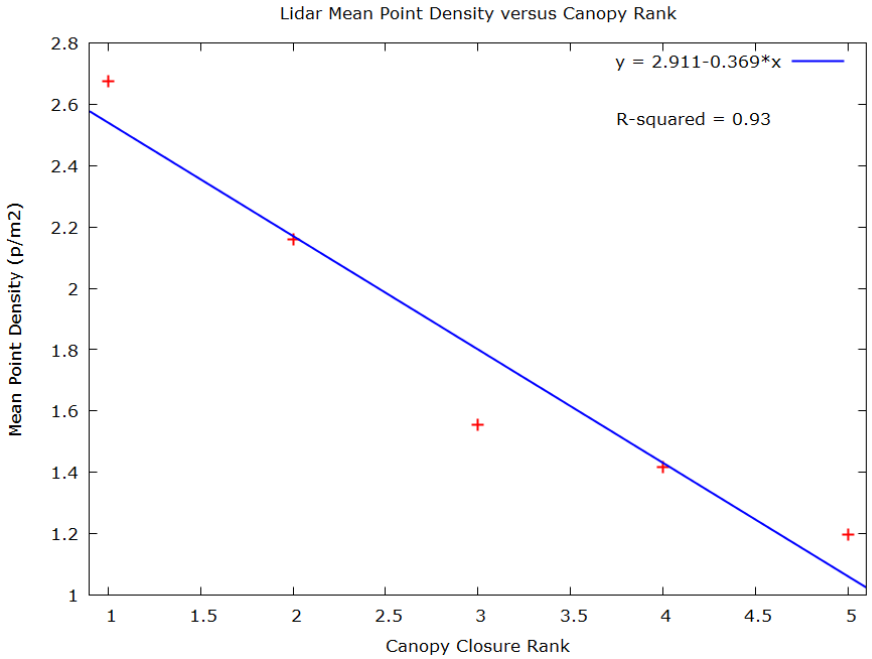

Figure 11: Lidar point density agreement with Canopy closure class rank

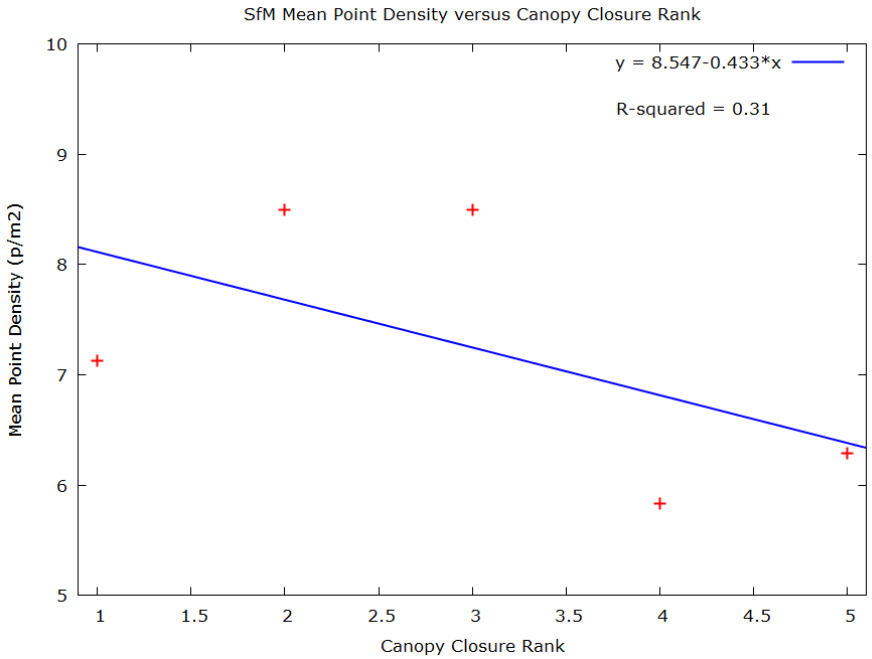

Figure 12: SfM point density agreement with Canopy closure class rank

4.3 Canopy Closure and DTM Error

While canopy closure exhibits some influence on mean point densities of both lidar and SfM datasets, it did not appear to influence DTM accuracy. No linear relationships are apparent between DTM accuracy (RMSE) and canopy closure estimates. Moreover, both lidar and SfM absolute error values are not normally distributed, violating an important assumption required by a linear model. Table 12 displays mean absolute differences in meters between each DTM and the GPS validation point at plot centroids. The standard deviation is italicized.

Table 6: DTM absolute mean error (meters) by canopy closure classification

DTM	NV	Very Low (12-26)	Low (27-41)	Medium (42-65)	High (66-78)
lidar NN 50cm	1.11	1.17	1.24	1.15	0.94
	0.07	*0.07*	*0.22*	*0.24*	*0.43*
SfM NN 50cm	0.60	0.93	1.58	2.07	1.41
	0.41	*0.50*	*1.02*	*1.11*	*0.77*
lidar NN 1m	1.11	1.17	1.22	1.14	0.89
	0.06	*0.07*	*0.24*	*0.25*	*0.46*
SfM NN 1m	0.60	0.93	1.58	2.07	1.41
	0.41	*0.50*	*1.02*	*1.11*	*0.77*
lidar NN 2m	1.11	1.17	1.24	1.15	0.94
	0.07	*0.09*	*0.19*	*0.25*	*0.47*
SfM NN 2m	0.59	0.90	1.35	1.75	1.39
	0.40	*0.54*	*0.84*	*1.36*	*0.81*
lidar Krig 1m	1.12	1.16	1.24	1.14	0.94
	0.08	*0.06*	*0.20*	*0.24*	*0.41*
SfM Krig 1m	0.59	0.88	1.60	1.84	1.38
	0.40	*0.54*	*0.81*	*1.28*	*0.80*

Generally, both DTM_{lidar} and DTM_{SfM} appear to be most accurate over non-vegetated plots, and exhibiting the highest absolute error under Low canopy closures. This trend does not continue, however. Under Medium and High canopy closures, the both DTM_{lidar} and DTM_{SfM} exhibit *lower* error, in some cases lower than the non-vegetated plots. For example, the 1-meter NN DTM_{lidar} has a mean error of 1.11 meters over non-vegetated plots, and 0.89 meters under High canopy closures. The 1-meter NN DTM_{SfM} is more accurate over non-vegetated plots than under High canopy closure, but the surface exhibits more error under Medium canopy closure (2.07 meters) than under High (1.41 meters), and follows the general trend of lower accuracy under denser canopy closures. There are several factors that may contribute to this result including interspecies canopy structure variability, interpolation of the surface from points not under canopy, and small sample size.

5. DISCUSSION

5.1 Influence of Canopy Closure, Interpolation, and Spatial Resolution

The goal of this study was to reconstruct a bare-earth DEM under different canopy conditions. Canopy closure was used to quantify the influence of vegetation on the model surface because it is a straightforward, easy to calculate metric that quantifies the amount of ground potentially visible from an aerial perspective. However, canopy closure did not appear to influence the DTM accuracy as expected. There are several possible reasons for this.

This study did not account for the variability of canopy closure between different tree species, nor did it attempt to model other, more complex structural metrics. For example, Wallace et al. (2016) calculated canopy cover directly from the SfM-derived point cloud, and validated estimates along transects over the entire study area (0.15 ha). Other canopy density estimation metrics could have potentially revealed underlying relationships, and should be investigated in future analysis.

Another possible reason for the lack of canopy influence on accuracy could be that the model surface under dense canopy is heavily interpolated from surrounding areas. Areas exhibiting high canopy closures and low topographic variability, may be entirely reconstructed from interpolated points not under the canopy, while surfaces under more moderate closures could be reconstructed largely from understory vegetation. Figure 12 shows the surrounding vegetation at a plot with relatively low mean slope (3.9º) that overestimated the GPS validation point by 1.79 meters with the 1-meter NN DTM_{SfM} and by 0.97 meters with the 1-meter NN DTM_{lidar}. The canopy closure estimate

for plot #2 is classified as Low with a 40 percent closure, which is only 1 percent less than the lowest value in the Medium class. Several other plots have similar low-lying vegetation that could have been misclassified as ground points.

Figure 13: Plot with low-lying vegetation

A structural metric that incorporates ground cover and low vegetation into the estimate would likely give a more complete view of how vegetation density influences model accuracy. Additionally, sampling the entire plot along a transect could potentially capture this information.

This study used two different interpolation methods to reconstruct DTM surfaces.

At 1-meter resolution, the DTM_{lidar} and DTM_{SfM} interpolated using Ordinary Kriging did not appear to have any substantial differences in accuracy compared with the Natural Neighbor method. The DTM_{SfM} had a slightly lower RMSE value with the Kriging method (1.58 meters) than with the NN (1.64 meters), and the DTM_{lidar} was less accurate by 1 centimeter. Both methods operate differently, but rely on inexact interpolation from points to sampled locations. The Natural Neighbor method was selected for this reason, and because it has been shown to work well on irregularly spaced and non-normally distributed data, and avoids creating abrupt surface changes and interpolation artifacts (Sibson, 1981). Comparison between an exact interpolation method such as Inverse Distance Weighting (IDW) would have likely provided greater contrast between models.

The 2-meter NN DTM_{SfM} was slightly more accurate than the 1-meter model, however, the 1-meter NN DTM_{lidar} had lower RMSE than the 2-meter model. While less dense, the ground-classified lidar point cloud was more regularly spaced than the SfM point cloud under canopy. This resulted in large gaps in the SfM points that required interpolation. At a coarser spatial resolution, the NN interpolated surface minimized the effect of outliers, and included more observed values in the model, slightly lowering the RMSE. This had a negligible effect on the more regularly-spaced lidar point cloud.

5.2 Ground Classification Method and Interpolated Surface

Although canopy closure and interpolation method did not appear to have any significant influence on DTM accuracy, an important factor that was not fully examined here is the ground classification algorithm. Because the DTM surface is generated directly from ground-classified points, the type of ground filter, as well as its parameters

are important considerations when attempting to reconstruct a bare-earth model. Similarly, decimation, automated outlier filtering parameters can have a potentially significant effect on the resulting DTM.

In this study, a morphological filtering algorithm was initially used to remove all points greater than 0.5 meters above the surface, and greater than 15 degrees from the nearest neighboring point within a 30-meter window, for each chunk (20 meters for the NE). It is possible that these parameters removed points that should have been classified as ground, resulting in large under-canopy gaps in the model. SfM is a passive sampling technique that is not capable of penetrating into canopy unless a gap is present. It is possible that the automated outlier filtering process removed some of these "lone" points that may have represented the actual surface beneath dense canopy or vegetation, excluding them from the DTM.

Although it is beyond the scope of this study, a comparison of different ground classification methods could potentially quantify the influence of method on SfM model accuracy. One example that should be investigated is the Cloth Simulation Filter (CSF), pioneered by Zhang et al. (2016) which operates by applying a mathematically-simulated rigid cloth to the inverted surface of the 3D point cloud. The algorithm then analyzes the interactions between the cloth nodes and the corresponding points, and the locations of the cloth nodes can be determined to generate an approximation of the ground surface.

While SfM point clouds do not include return information, the points do contain scalar information from the original images (i.e. R,G,B). With the inclusion of NIR, it should be possible to develop a classification method that incorporates derived vegetation indices to filter out canopy.

Another possible method of ground classification is the application of a multiscale dimensionality criterion that operates by characterizing the local 3D organization of the point cloud within an adaptive spherical window around each point. This approach was demonstrated to achieve 98 percent accuracies when separating vegetation from ground in mountain riparian environments, and could be investigated over this study area (Brodu and Lague, 2012).

5.3 SfM Limitations

One of the objectives of this analysis was to document the limitations of using the SfM method to generate bare-earth DEMs under specific conditions. As noted previously, aerial imagery was collected in 4 sections covering roughly equal areas of the study area. Imagery covering the SE section, was acquired under different illumination conditions due to loss of cloud cover. This resulted in alignment errors with other sections at areas of overlap and non-linear deformation of the merged point cloud. The SE section exhibited errors of nearly 4 meters in some overlapping areas. Figures 14-17 illustrate the deformation, and observed overestimation of vertical point-to-point distances.

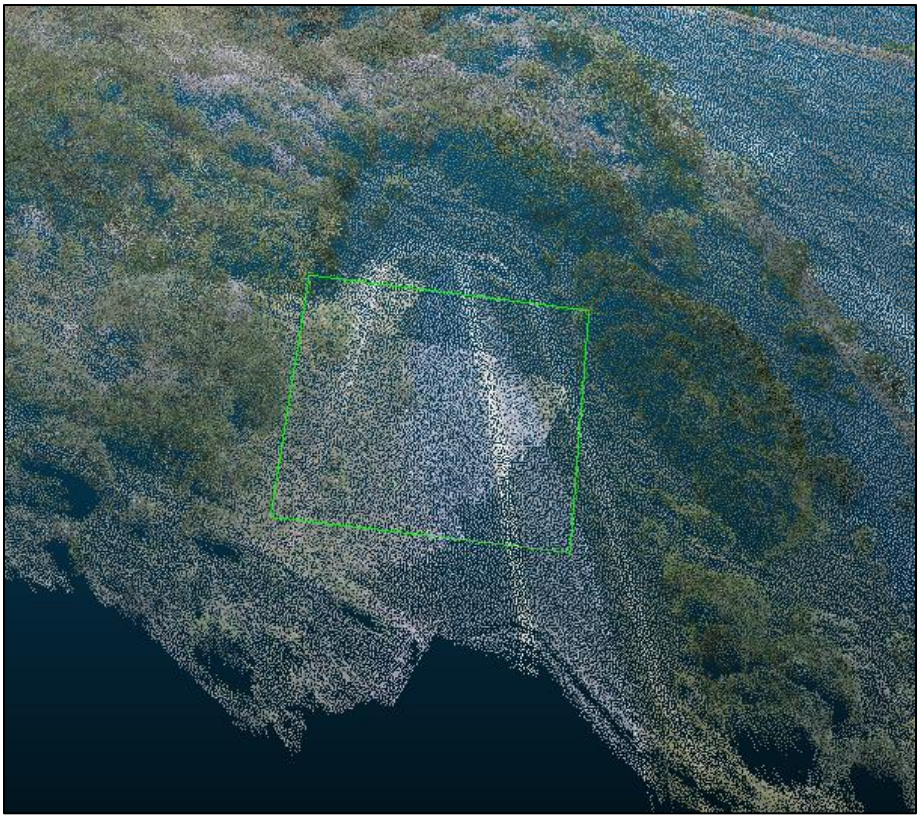

Figure 14: Misalignment along overlapping sections of SfM clouds

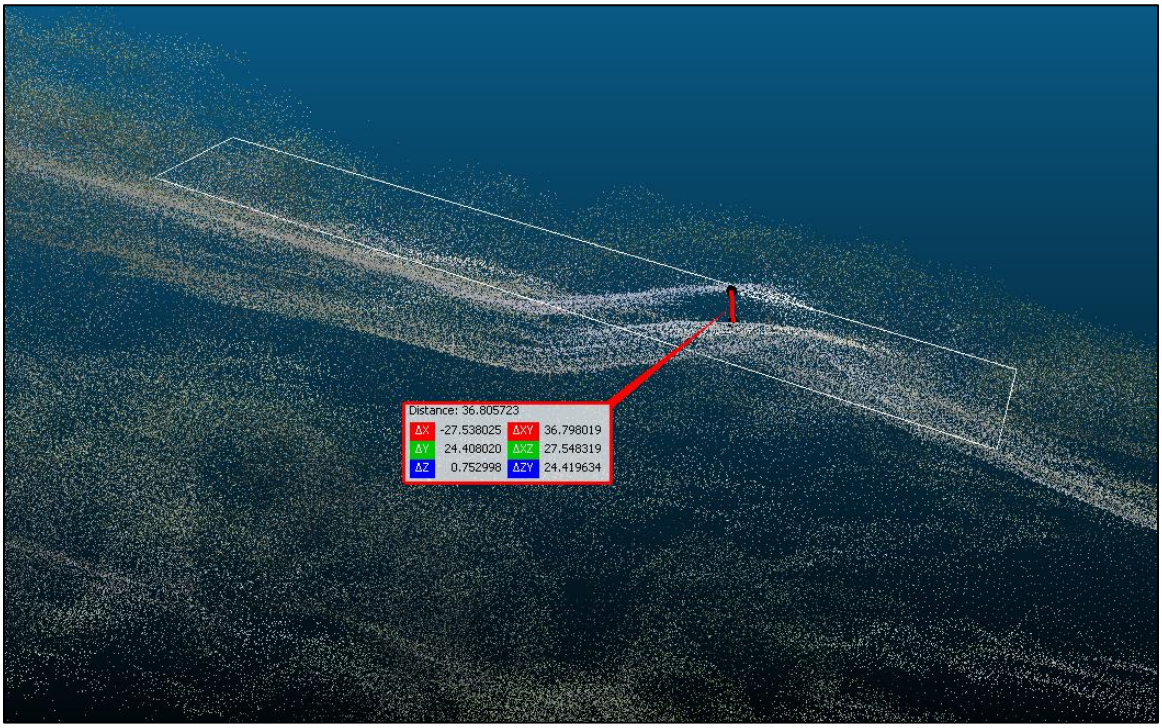

Figure 15: Oblique view of area depicted in Fig. 13 (distance is 3.68 meters)

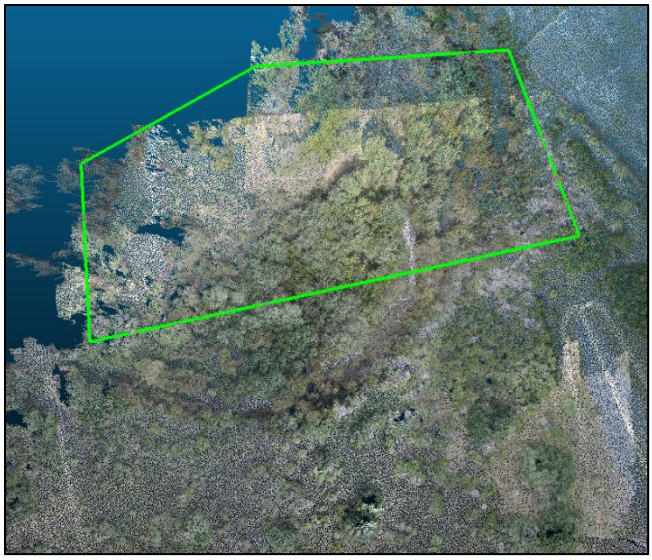

Figure 16: Misalignment along another overlapping section of SfM clouds

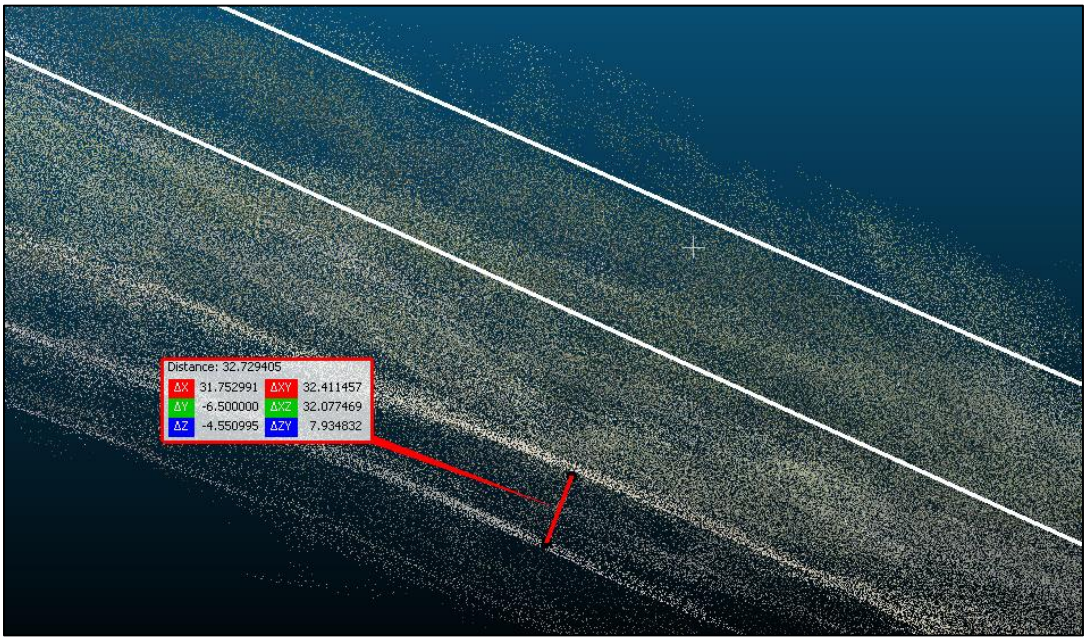

Figure 17: Oblique view of area depicted in Fig. 16 (distance is 3.27 meters)

Attempts to properly align the SE section using a matrix transformation based on an Iterative Closest Point (ICP) point-matching algorithm were unsuccessful because the

deformation was not linear (i.e. spatially inconsistent). The overall result of this deformation was greater RMSE in all DTM_{SfM} than DTM_{lidar}, especially in plots spatially coincident with section overlap. Some amount of the observed model error may be due to edge-warping around section perimeters. Szpakowski (2016) observed similar edge-warping over a 0.48 ha study area, however, these areas also overlap the SE section, so it was difficult to determine the degree to which edge-warping affected DTM error in these locations.

Reprocessing the original imagery as a single chunk, could potentially separate edge-warping effects from the non-linear deformation artifacts although this would require much more processing time and greater computational resources (i.e. RAM). Dandois and Ellis (2015) note that radiometric corrections may be useful to reduce the influence of variable scene lighting on model accuracy when it is not possible to collect images under constant lighting conditions.

Several factors influence the choice of flight altitude, including the resolution of the GoPro camera used to acquire imagery. The 7-megapixel resolution required that the flight altitude remain relatively low over a 22-ha study area to maximize image resolution for feature detection, as well as achieve adequate image overlap. This produced a large number of images, resulting in a very dense point cloud which was difficult to work with given the computational resources. James and Robson (2014) note that the collection of fewer, more oblique images can reduce DEM deformation and systematic error by two orders of magnitude. Future research over this or similar sites should reduce the number of images generated by increasing the flight altitude and sensor resolution, and collecting several off-nadir images per flight line.

6. CONCLUSION

This study investigated the use of SfM for DTM generation and assessed the accuracy of the resulting bare-earth surfaces under increasing canopy densities. This was compared with an existing lidar-generated model at three different spatial resolutions, using two interpolation methods. The results indicate that the lidar-generated DTM was more accurate than the SfM-generated DTM at all spatial resolutions. In this study, canopy closure was not demonstrated to be a strong predictor of model accuracy in either the SfM or lidar DTM. While the SfM model accuracy was certainly influenced by non-linear deformation, the accuracy of the undistorted lidar model was not influenced by canopy closure estimates following any observed linear trends. Future research should continue to investigate and quantify this relationship.

LITERATURE CITED

Arya, Sunil, David M. Mount, Nathan S. Netanyahu, Ruth Silverman, and Angela Y. Wu. "An optimal algorithm for approximate nearest neighbor searching fixed dimensions." *Journal of the ACM (JACM)* 45, no. 6 (1998): 891-923.

"ASPRS Positional Accuracy Standards for Digital Geospatial Data." *Photogrammetric Engineering & Remote Sensing* 81, no. 3 (March 2015): A1-A26. doi:10.14358/PERS.81.3.A1-A26.

Bishop, T. F. A., and A. B. McBratney. "Creating field extent digital elevation models for precision agriculture." *Precision Agriculture* 3, no. 1 (2002): 37-46.

Bonner, W. J., and R. A. Schmall. *A photometric technique for determining planetary slopes from orbital photographs.* No. 812-A. 1973.

Brodu, Nicolas, and Dimitri Lague. "3D terrestrial lidar data classification of complex natural scenes using a multi-scale dimensionality criterion: Applications in geomorphology." *ISPRS Journal of Photogrammetry and Remote Sensing* 68 (2012): 121-134.

Chirico, Peter G., Katherine C. Malpeli, and Sarah M. Trimble. "Accuracy evaluation of an ASTER-derived global digital elevation model (GDEM) version 1 and version 2 for two sites in western Africa." *GIScience & Remote Sensing* 49, no. 6 (2012): 775-801.

Dandois, Jonathan P., and Erle C. Ellis. "Remote sensing of vegetation structure using computer vision." *Remote Sensing* 2, no. 4 (2010): 1157-1176.

Dandois, Jonathan P., Marc Olano, and Erle C. Ellis. "Optimal altitude, overlap, and weather conditions for computer vision UAV estimates of forest structure." *Remote Sensing* 7, no. 10 (2015): 13895-13920.

Deilami, Kaveh, and Mazlan Hashim. "Very high resolution optical satellites for DEM generation: a review." *European Journal of Scientific Research* 49, no. 4 (2011): 542-554.

DeWitt, J. D., T. A. Warner, and J. F. Conley. "Comparison of DEMS derived from USGS DLG, SRTM, a statewide photogrammetry program, ASTER GDEM and LiDAR: implications for change detection." *GIScience & Remote Sensing* 52, no. 2 (2015): 179-197.

Dietrich, James T. "Riverscape mapping with helicopter-based Structure-from-Motion photogrammetry." *Geomorphology* 252 (2016): 144-157.

Dixon, Richard. "Climatology of the Freeman Ranch, Hays County, Texas." *Free Ranch Publ Ser* 3 (2000): 1-9.

Edelsbrunner, Herbert, and Ernst P. Mücke. "Three-dimensional alpha shapes." *ACM Transactions on Graphics (TOG)* 13, no. 1 (1994): 43-72.

Egan, D. "Fact sheet: Canopy cover and canopy closure." Ecological Restoration Institute Fact Sheet (2010)

Fischler, Martin A., and Robert C. Bolles. "Random sample consensus: a paradigm for model fitting with applications to image analysis and automated cartography." *Communications of the ACM* 24, no. 6 (1981): 381-395.

Fonstad, Mark A., James T. Dietrich, Brittany C. Courville, Jennifer L. Jensen, and Patrice E. Carbonneau. "Topographic structure from motion: a new development in photogrammetric measurement." *Earth Surface Processes and Landforms* 38, no. 4 (2013): 421-430.

Furukawa, Yasutaka, and Jean Ponce. "Accurate, dense, and robust multiview stereopsis." *IEEE transactions on pattern analysis and machine intelligence* 32, no. 8 (2010): 1362-1376.

Gesch, Dean B., Michael J. Oimoen, and Gayla A. Evans. *Accuracy assessment of the US Geological Survey National Elevation Dataset, and comparison with other large-area elevation datasets: SRTM and ASTER*. No. 2014-1008. US Geological Survey, 2014.

Griffith, G., S. Bryce, J. Omernik, and A. Rogers. "Ecoregions of Texas. Texas Commission on Environmental Quality." (2007).

Hengl, T., Evans, I.S. "Mathematical and Digital Models of the Land Surface." In *Geomorphometry: Concepts, Software, and Applications.* edited by Hengl, T., Reuter, H.I. pp. Amsterdam: Elsevier, 2009.

Hensley, S., R. Munjy, and P. Rosen. 2007. “Interferometric Synthetic Aperture Radar, Digital Elevation Model Technologies and Applications.” Chapter 6. In *The DEM User’s Manual*, edited by D. F. Maune, 142–206. Bethesda, MD: ASPRS.

Hulet, April, Bruce A. Roundy, Steven L. Petersen, Stephen C. Bunting, Ryan R. Jensen, and Darrell B. Roundy. "Utilizing national agriculture imagery program data to estimate tree cover and biomass of pinon and juniper woodlands." *Rangeland Ecology & Management* 67, no. 5 (2014): 563-572.

Hutchinson, Michael, and John C. Gallant. "Digital elevation models and representation of terrain shape." In *Terrain Analysis: Principles and Applications*. John Wiley & Sons (2000).

Isioye, O. A., P. Jobin, and T. T. Youngu. "An assessment of digital elevation models (DEMs) from different spatial data sources." *Asian Journal of Engineering, Sciences & Technology* 2, no. 1 (2012).

James, M. R., and Stuart Robson. "Straightforward reconstruction of 3D surfaces and topography with a camera: Accuracy and geoscience application." *Journal of Geophysical Research: Earth Surface* 117, no. F3 (2012).

Javernick, L., J. Brasington, and B. Caruso. "Modeling the topography of shallow braided rivers using Structure-from-Motion photogrammetry." *Geomorphology* 213 (2014): 166-182.

Jennings, S. B., N. D. Brown, and D. Sheil. "Assessing forest canopies and understorey illumination: canopy closure, canopy cover and other measures." *Forestry* 72, no. 1 (1999): 59-74.

Jensen, Jennifer LR, and Adam J. Mathews. "Assessment of image-based point cloud products to generate a bare earth surface and estimate canopy heights in a woodland ecosystem." *Remote Sensing* 8, no. 1 (2016): 50.

Kraus, Karl, and Norbert Pfeifer. "Determination of terrain models in wooded areas with airborne laser scanner data." *ISPRS Journal of Photogrammetry and Remote Sensing* 53, no. 4 (1998): 193-203.

Kuebler, Daniel, Patrick Hildebrandt, Sven Guenter, Bernd Stimm, Michael Weber, Reinhard Mosandl, Johana Munoz et al. "Assessing the importance of topographic variables for the spatial distribution of tree species in a tropical mountain environment." *ERDKUNDE* 70, no. 1 (2016): 19-47.

Liu, Xiaoye. "Airborne LiDAR for DEM generation: some critical issues." *Progress in Physical Geography* 32, no. 1 (2008): 31-49.

Lohr, U. "Digital Elevation Models by Laserscanning." In *Coastal and Marine Geo-Information Systems*, pp. 349-354. Springer Netherlands, 2003.

Lowe, David G. "Distinctive image features from scale-invariant keypoints." *International journal of computer vision* 60, no. 2 (2004): 91-110.

Maguya, Almasi S., Virpi Junttila, and Tuomo Kauranne. "Algorithm for extracting digital terrain models under forest canopy from airborne LiDAR data." *Remote Sensing* 6, no. 7 (2014): 6524-6548.

Mathews, Adam J., and Jennifer LR Jensen. "Visualizing and quantifying vineyard canopy LAI using an unmanned aerial vehicle (UAV) collected high density structure from motion point cloud." *Remote Sensing* 5, no. 5 (2013): 2164-2183.

Maune, David Francis, ed. *Digital elevation model technologies and applications: the DEM user's manual*. Asprs Publications, 2007.

Meng, Xuelian, Nate Currit, and Kaiguang Zhao. "Ground filtering algorithms for airborne LiDAR data: A review of critical issues." *Remote Sensing* 2, no. 3 (2010): 833-860.

Miller, Charles Leslie, and Robert Arthur Laflamme. *The Digital Terrain Model-: Theory & Application.* MIT Photogrammetry Laboratory, 1958.

Mutlu, Muge, Sorin C. Popescu, and Kaiguang Zhao. "Sensitivity analysis of fire behavior modeling with LIDAR-derived surface fuel maps." *Forest Ecology and Management* 256, no. 3 (2008): 289-294.

Nelson, A., Reuter, H.I., Gessler, P. DEM production methods and sources. In: Hengl, T., Reuter, H.I. (Eds.), *Geomorphometry: Concepts, Software, and Applications*. Elsevier, Amsterdam, (2009) 65–85.

Newton, B. Talon, Ethan Mamer, Peter ReVelle, and Hector Garduño. "Sacramento Mountains Watershed Study–The Effects of Tree Thinning on the Local Hydrologic System." (2015).

Ouédraogo, Mohamar Moussa, Aurore Degré, Charles Debouche, and Jonathan Lisein. "The evaluation of unmanned aerial system-based photogrammetry and terrestrial laser scanning to generate DEMs of agricultural watersheds." *Geomorphology* 214 (2014): 339-355.

Perko, R., H. Raggam, K. H. Gutjahr, and M. Schardt. "Advanced DTM generation from very high resolution satellite stereo images*." ISPRS Annals of the Photogrammetry, Remote Sensing and Spatial Information Sciences* 2, no. 3 (2015): 165.

Pike, R.J., Evans, I.S., Hengl, T. "Mathematical and Digital Models of the Land Surface." In: Hengl, T., Reuter, H.I. (Eds.), *Geomorphometry: Concepts, Software, and Applications*. Elsevier, Amsterdam, (2009) 3-30.

Pike, Richard J., and Stephen E. Wilson. "Elevation-relief ratio, hypsometric integral, and geomorphic area-altitude analysis." *Geological Society of America Bulletin* 82, no. 4 (1971): 1079-1084.

Pirokka, M., E.C. Ellis, and P.D. Tredici. "Personal Remote Sensing: Computer Vision Landscapes." In A. Fard and T. Meshkani, editors. *New Geographies #7: Geographies of Information*. Harvard Graduate School of Design, Cambridge, MA.: (2015) 178-187

Sesnie, Steven E., Paul E. Gessler, Bryan Finegan, and Sirpa Thessler. "Integrating Landsat TM and SRTM-DEM derived variables with decision trees for habitat classification and change detection in complex neotropical environments." *Remote Sensing of Environment* 112, no. 5 (2008): 2145-2159.

Shen, Z. Y., L. Chen, Q. Liao, R. M. Liu, and Q. Huang. "A comprehensive study of the effect of GIS data on hydrology and non-point source pollution modeling." *Agricultural water management* 118 (2013): 93-102.

Snavely, Noah, Steven M. Seitz, and Richard Szeliski. "Modeling the world from internet photo collections." *International Journal of Computer Vision* 80, no. 2 (2008): 189-210.

Szpakowski, D. (2016). Estimating aboveground biomass of pasture environments using structure from motion (Master's thesis). Retrieved from https://digital.library.txstate.edu/bitstream/handle/10877/6308/SZPAKOWSKI-THESIS-2016.pdf

Sibson, Robin. "A brief description of natural neighbour interpolation." *Interpreting multivariate data* 21 (1981): 21-36.

Tarekegn, Tesfaye Haimanot, Alemseged Tamiru Haile, Tom Rientjes, P. Reggiani, and Dinand Alkema. "Assessment of an ASTER-generated DEM for 2D hydrodynamic flood modeling." *International Journal of Applied Earth Observation and Geoinformation* 12, no. 6 (2010): 457-465.

Véga, Cédric, and Benoît St-Onge. "Mapping site index and age by linking a time series of canopy height models with growth curves." *Forest Ecology and Management* 257, no. 3 (2009): 951-959.

Wallace, Luke. "Assessing the stability of canopy maps produced from UAV-LiDAR data." In 2013 *IEEE International Geoscience and Remote Sensing Symposium-IGARSS*, pp. 3879-3882. IEEE, 2013.

Wallace, Luke, Arko Lucieer, Zbyněk Malenovský, Darren Turner, and Petr Vopěnka. "Assessment of Forest Structure Using Two UAV Techniques: A Comparison of Airborne Laser Scanning and Structure from Motion (SfM) Point Clouds." *Forests* 7, no. 3 (2016): 62.

Westoby, M. J., J. Brasington, N. F. Glasser, M. J. Hambrey, and J. M. Reynolds. "'Structure-from-Motion'photogrammetry: A low-cost, effective tool for geoscience applications." *Geomorphology* 179 (2012): 300-314.

Winn, Matthew, Jeff Palmer, S-M. Lee, and Philip Araman. "ForestCrowns: a transparency estimation tool for digital photographs of forest canopies." (2016).

Shen, Z. Y., L. Chen, Q. Liao, R. M. Liu, and Q. Huang. "A comprehensive study of the effect of GIS data on hydrology and non-point source pollution modeling." *Agricultural water management* 118 (2013): 93-102.

White, Joanne C., Michael A. Wulder, Mikko Vastaranta, Nicholas C. Coops, Doug Pitt, and Murray Woods. "The utility of image-based point clouds for forest inventory: A comparison with airborne laser scanning." *Forests* 4, no. 3 (2013): 518-536.

Zhang, Keqi, Shu-Ching Chen, Dean Whitman, Mei-Ling Shyu, Jianhua Yan, and Chengcui Zhang. "A progressive morphological filter for removing nonground measurements from airborne LIDAR data." *IEEE Transactions on Geoscience and Remote Sensing* 41, no.4 (2003): 872-882.

Zhang, K., and Z. Cui. "ALDPAT 1.0. Airborne LIDAR Data processing and Analysis Tools." *National Center for Airborne Laser mapping. Florida International university* (2007).